

POLITECNICO DI TORINO

Master's Degree in Automotive Engineering

AY 2022/2023

April 2023

Characterization of Metal-Filled Resin for Stereolithography

Relatori:

Prof.ssa Eleonora Atzeni

Ing. Wadiah Yared

Candidato:

Massimo Surace

I. Preface

The present work has been developed in the Institute for Manufacturing Technologies of Ceramic and Composite Component (IMTCCC) of the University of Stuttgart.

The IMTCC is focused on research topics in manufacturing techniques for ceramic components and composites as well as in material technology. The main research scope is the interaction between modern material science, process engineering and manufacturing technologies. The structural, functional and lightweight solutions, as well as the high-performance coatings, are projected toward several fields of application such as the automotive and aerospace, medical, mechanical and energy and power plant industries.

In the institute, stereolithography is used in combination with ceramic filled resin to produce lightweight and customized products for medical application. The methodologies and testing procedures adopted in this work are therefore strictly related to the know-how of the institute that provided me with the proper knowledge on the ceramic-filled resin for stereolithography. All the necessary equipment was also kindly provided by the institute.

II. Abstract

The objective of this work is the characterization of a UV-curable metal-filled resin suitable for the production of metal components with an additive manufacturing process based on stereolithography. The major focus is given to the integration of an aluminium alloy powder into an acrylic resin curable through irradiation of light with wavelength equal to 405 nm. Different powders are considered and their effects on suspension stability and curing kinetics are analyzed with rheology and photo-rheology tests. The air trapping phenomenon has been investigated and reduced with a vacuum mixer. Moreover, some defoamer have been tested. The suspension stability and the resin viscosity have been adjusted by balancing the base resin composition and with the integration of proper rheological additives. After the stabilization of the suspension, the printing parameters for the filled resin have been determined experimentally, and some green parts have been produced and analyzed at the microscope. Considerations about debinding and sintering steps are made.

The metal-filled resin resulted to be a viable path for the production of green parts with stereolithography and a good opportunity for the development of an alternative AM technology for metal components.

III. Index

I. Preface.....	I
II. Abstract	III
III. Index.....	IV
IV. List of Figures	VI
V. List of Tables.....	VIII
VI. Abbreviations	IX
1. Introduction.....	1
1.1. Basic concepts of AM.....	1
1.2. Direct and indirect AM processes for metals.....	3
1.2.1. L-PBF	4
1.2.2. EBM	5
1.2.3. DED.....	6
1.2.4. ADAM and BMD	7
1.2.5. Metal Jet	8
2. State of the art	10
2.1. Stereolithography.....	10
2.2. Free and constrained surface layout.....	11
2.3. Irradiation techniques for SLA	13
2.3.1. Laser-SLA	13
2.3.2. Masked-SLA.....	14
2.3.3. DLP-SLA.....	15
2.4. Resin for SLA	17
2.4.1. Precursors	18
2.4.2. Photoinitiator	19
2.4.3. Fillers.....	20
2.5. Filled resin for SLA	20
2.5.1. Scattering of light	21

2.5.2.	Dispersants	22
3.	Experimental implementation	25
3.1.	The printer.....	25
3.2.	Analysis of the powders.....	26
3.3.	Critical aspects for resin printability.....	26
3.3.1.	Suspension stability	27
3.3.2.	Powder-light interaction	28
3.3.3.	Air pockets.....	29
3.4.	Printing parameters	30
3.4.1.	Exposure time of the first layer	30
3.4.2.	Exposure time	31
3.4.3.	Layer height.....	31
3.4.4.	Tilt time	31
3.5.	Debinding and sintering.....	32
4.	Results and discussion.....	33
4.1.	Powder characterization.....	33
4.1.1.	Particle Size Distribution.....	33
4.1.2.	Particle morphology	34
4.2.	Curing kinetics	37
4.2.1.	Effects of the filler on curing behavior.....	37
4.2.2.	Air pockets.....	41
4.3.	Suspension stability and resin viscosity.....	44
4.3.1.	Effect of different powders on sedimentation	44
4.3.2.	Rheology additives	46
4.3.3.	Definition of an optimized formulation.....	49
4.4.	Optimization of printing parameters.....	52
4.5.	Debinding and sintering.....	55
5.	Conclusion.....	57
	References.....	59

IV. List of Figures

Figure 1. Main steps of an AM process.....	2
Figure 2. LPBF production steps.....	4
Figure 3. Schematic of a DED machine with electron beam power source.....	6
Figure 4. Schematic of an FDM machine	8
Figure 5. HP Metal Jet working principle [11].....	9
Figure 6. Workflow of indirect AM techniques.....	9
Figure 7. Different setup of H. Kodama SL machines	11
Figure 8. Free (a) and constrained (b) surface layout for SLA adapted from [15].....	12
Figure 9. Laser-SLA setup [18].....	13
Figure 10. Components of a MSLA printer	15
Figure 11. Comparison between LCD (a) and DLP (b)	16
Figure 12. Resin for SLA [14].....	18
Figure 13. Acrylate ion (a) and epoxyde cyclic ether (b).....	19
Figure 14. Rayleigh and Mie scattering [29].....	21
Figure 15. Potential curves of particles attraction and repulsion [30].....	23
Figure 16. Electric stabilization (a) and steric stabilization (b) [31].....	24
Figure 17. Prusa SL1S printer	25
Figure 18. Laser diffraction particle size analyzer	26
Figure 19. Rheometer with parallel plate configuration.....	27
Figure 20. Photo-rheology setup	28
Figure 21. Smartphone holder for microscope videorecording.....	29
Figure 22. Example of a component without pad (a) and with pad (b).....	30
Figure 23. PSD of the used powder	33
Figure 24. Micrograph of AlSi10Mg powder in acrylic resin.....	35
Figure 25. Micrograph of sieved AlSi10Mg powder in acrylic resin.....	35
Figure 26. Micrograph of Al ₂ O ₃ powder in acrylic resin	36
Figure 27. SEM micrograph of 316L powder	36
Figure 28. SEM micrograph of AlSi12 powder	37

Figure 29. Photo-rheology curve of resin filled with AlSi10Mg powder	38
Figure 30. PR curves of resin filled with AlSi12Mg and Al ₂ O ₃ powder.....	39
Figure 31. PR curves of vacuum mixed resin filled with AlSi10Mg particles.....	41
Figure 32. Micrograph of an air pocket with the focus at different depth.....	42
Figure 33. Single cured layer of filled resin mixed without (a) and with (b) vacuum ...	43
Figure 34. AlSi10Mg (a) and Al ₂ O ₃ (b) powder suspension in acrylic resin	44
Figure 35. AlSi12 powder suspension in acrylic resin	45
Figure 36. 316L powder sedimented in acrylic resin	45
Figure 37. Amplitude sweep curves for different dispersants	48
Figure 38. Frequency sweep curves for different dispersants	48
Figure 39. Viscosity vs shear-rate for filled resin with different dispersants.....	49
Figure 40. Amplitude sweep curves for the optimized resin with BYK-P2720.....	51
Figure 41. Frequency sweep curves for the optimized resin with BYK-P2720.....	51
Figure 42. Viscosity vs shear-rate tuning the GARAMITE-1210 content.....	52
Figure 43. Micrograph of a printed part made of multiple layers	53
Figure 44. Micrograph of the sawtooth profile of a printed part.....	54
Figure 45. Micrograph of a printed part	54
Figure 46. Green part (a) and debinded part in oxidizing environment (b).....	55
Figure 47. Brown bodies with filling ratios equal to 30 (a) and 50 (b) wt%.....	56

V. List of Tables

Table 1. Values of D10, D50 and D90 of the examined powders.....	34
Table 2. Cure depth of a resin with increasing AlSi10Mg powder content	39
Table 3. Cure depth of an Al ₂ O ₃ powder filled resin with increasing mixing energy.....	40
Table 4. Vacuum mixing effect on cure depth of filled resin.....	42
Table 5. Tested defoamers.....	43
Table 6. Powder densities.....	44
Table 7. Effects of dispersants on suspension stability and viscosity	47
Table 8. Boosters	50
Table 9. Optimized printing parameters	53
Table 10. average shrinkage of parts after debinding for different filling ratio	56

VI. Abbreviations

Abbreviation	Description
AM	Additive Manufacturing
BJ	Binder Jetting
CAD	Computer-Aided Design
CAE	Computer-Aided Engineering
CFD	Computational Fluid Dynamics
CLIP	Continuous Liquid Interface Production
DED	Directed Energy Deposition
DLP	Digital Light Processing
DMD	Digital Micromirror Device
EBM	Electron Beam Melting
FDM	Fused Deposition Modelling
FEA	Finite Element Analysis
L-PBF	Laser Powder Bed Fusion
LCD	Liquid Crystal Display
MJ	Metal Jetting
MSLA	Masked Stereolithography
PBF	Powder Bed Fusion
PI	Photoinitiator
PR	Photo-Rheology
PSD	Particle Size Distribution
SEM	Scanning Electron Microscope
SLA	Stereolithography Apparatus
SLM	Selective Laser Melting
TPP	Two Photon Polymerization
UV	Ultra-Violet
VPP	Vat Photopolymerization

1. Introduction

An innovative *Additive Manufacturing* (AM) technology for the production of optimized lightweight components is explored in this work. The objective is the characterization of a metal-filled UV-curable resin suitable for a *Stereolithography* (SLA) technique and the definition of the printing, debinding and sintering parameters needed for the realization of a defect-free final component.

In the digital era, the interest toward AM techniques is growing for their ability of increasing design freedom and minimizing the raw material consumption. Among the main advantages of AM, we can mention the possibility of producing lightweight components and integrated assemblies in a single manufacturing step generating complex shapes that are not feasible via conventional subtractive technologies. Furthermore, the production of components doesn't require any specific tooling and can be concluded in few hours directly from the 3D *Computer-Aided Design* (CAD) model. These features are relevant in a variety of engineering applications such as the aerospace, the automotive and racing, biomedical, but also in architecture, design and jewelry and many other fields. On the other side, this kind of technologies still present many criticalities that are mainly related to the production speed and volume, to the material availability, to the surface quality and the parts defect, and the post processing labor requirement. The importance of developing new production processes is therefore related to the possibility to overcome some of these drawbacks for specific applications. In the case study of this project, the intent is to exploit the peculiarities of *Masked SLA* (MSLA) to produce metal components. Being an indirect AM process, MSLA may indeed allow the production of materials not printable with the conventional AM technologies used to produce metal parts such as the *Laser Powder Bed Fusion* (L-PBF) and the *Electron Beam Melting* (EBM) [1].

1.1. Basic concepts of AM

The basic principle behind additive manufacturing is the realization of components in an additive fashion with the extensive use of informatic software able to produce a suitable

algorithm for the machine (hereafter “*printer*”) starting from the 3D CAD model [2]. The vast majority of the AM technologies available today are based on the concept of *Layered Manufacturing*, i.e., the part is “*sliced*” in many different layers of defined height by a software referred to as the ‘*slicer*’ and then the instructions for the production of each layer are delivered to the printer that generates the entire object in a layer-by-layer manufacturing process (Figure 1).

To exploit the full potential of AM, the 3D model could be optimized and adapted to the available technology using *Computer-Aided Engineering* (CAE) software able to perform *topological or genetic optimization* and generate organic structures to withstand the expected stresses that the part will face during his working life. Common simulation modeling techniques include *Computational Fluid Dynamics* (CFD), *Finite Element Analysis* (FEA), and *Non-Linear Stress Analysis*. Following that, the net shape of the component is translated into a file format suitable to be read by the slicer (mainly .STL) that, most of the times, is also able to generate the support structure needed during the production of overhangs and inclined surfaces. The .STL file uses triangles to describe the geometry of the object, therefore the translation implies a loss of accuracy and sometimes also conversion errors (errors in .STL files can almost always be automatically fixed in the slicing software). The output file from the slicer (G-Code) contains all the instructions and printing parameters to produce the component and it is given to the printer that can start the physical fabrication of the part. When the print is over, depending on the technology used and on the final part application support removal and post-processing operation are performed. This last step is critical since it often requires tedious manual work and skills of the operator with a negative effect on production cost and speed.

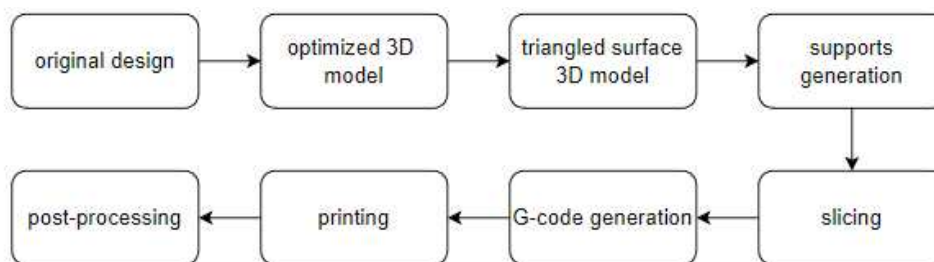


Figure 1. Main steps of an AM process

1.2. Direct and indirect AM processes for metals

Due to the inefficiency and low power of the energy sources, the earliest metal AM machines were only able to process metallic powders mixed with a polymeric binder. These machines were considered indirect manufacturing systems because post-treatments were necessary to obtain an all-metal part with good mechanical performances [3]. Nowadays, the production of metal AM parts can be directly achieved by sintering or melting a metal powder or wire. In this case the material supplied to the machine is the same as the final part that, after a thermal process, features specific characteristics depending on the process itself and the process parameters. The thermal power is usually provided by a laser or an electron beam such as in the cases of the afore-mentioned L-PBF and EBM but also other technologies directly melt metal powders or wires such as the wire and powder *Directed Energy Deposition* (DED) and the *Joule Printing*. The key of the success of these technologies is in the single step manufacturing process that implies the usage of a single machine for the entire production of the part. Nonetheless, the as-printed part has then to be post-processed to achieve the net shape and desired tolerances and roughness and this step involves machining and other operations on hard metal components.

Due to their complexity and the high requirements in terms of power to melt the metals, the machines of conventional AM techniques can be expensive. Moreover, the production of parts with internal cavities is not feasible with powder bed-based processes because the unprocessed powder needs to be removed by mechanical or manual operations and these cavities are not accessible after the printing [3]. Furthermore, the handling of powders may require special attention to take care for the health of the operators. To reduce the cost, improve safety and increase the range of printable materials, some new indirect AM techniques have been developed, among them we can mention: *Bound Metal Deposition* (BMD) patented by Desktop Metal, *Atomic Diffusion Additive Manufacturing* (ADAM) patented by Markforged and *Metal Jet* (MJ) patented by HP [4, 5].

1.2.1. L-PBF

The L-PBF, also known as *Selective Laser Melting* (SLM), is a layer-based AM technique in which a powder bed is melted selectively by a laser. The machine consists of a movable building platform that is coated with a fine metal powder by a recoater blade. When the powder is evenly spread on the entire building platform, one or more laser beams melt the metal powder to produce a solid layer firmly attached to the platform. Once the first layer is completed, the platform is moved of a distance equal to the layer height and the new layer can be printed in the same manner. At the end of the process, all the excess powder in the build volume is removed and the parts are revealed [6].

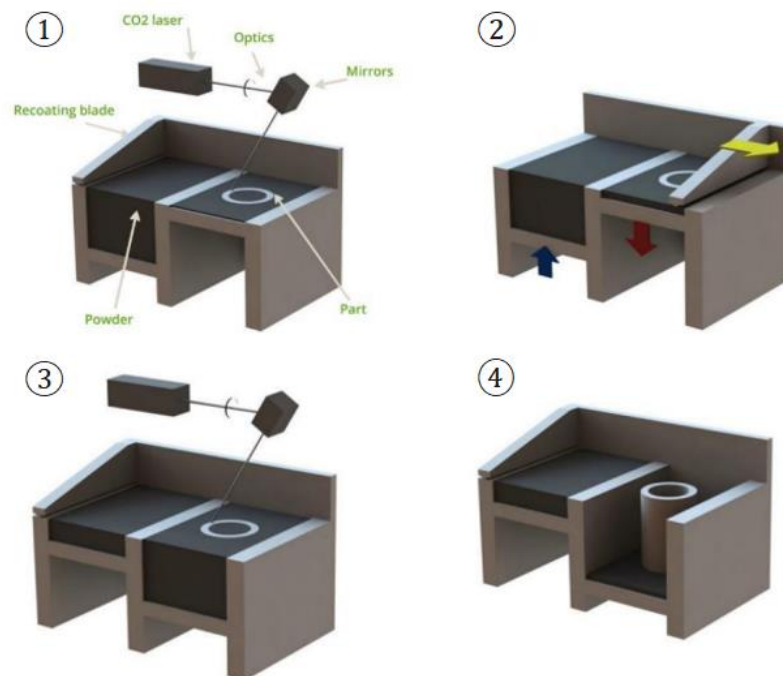


Figure 2. LPBF production steps¹

- ① the laser irradiates the powder, ② the platform lowers of one layer and the recoater spreads the powder, ③ step 1 and 2 are repeated until the part is complete, ④ the excess powder is removed from the build volume

¹ Image adapted from [6]

At the end of the production, the parts are annealed in a furnace to reduce thermal stresses. After that, wire cutting is commonly adopted to separate the parts from the build platform and the residual material on the platform is then removed in machining operation [6]. The design freedom guaranteed by LPBF and the good variety of metal powders available, mainly steels, Ti alloys, Inconel and Al alloys, make this technology optimal for the production of optimized and lightweight components. Nonetheless, some foresights have to be followed to minimize thermal strain and support structures. Moreover, enclosed cavities are not feasible due to the powder trapping. In terms of printing speed, it is limited by the galvanometer movements, but this limitation can be partially overcome by the utilization of multiple lasers. The energy and raw material consumption are related to the high power required by the laser beams and to the part volume. Furthermore, an inert gas, usually nitrogen or argon, is used to avoid oxidation of the metal at high temperature during the process. Also, the excess powder in the build volume can be recycled and reused for another print taking care of the impurities produced during the production [7].

1.2.2. EBM

Similarly to LPBF, also EBM is a powder bed AM technology using an electron beam as a power source. Being without any moving part, the electron beam can be efficiently moved at translational speed up to 1000 times faster than the laser beam (8000 m/s) [7] and the temperatures reached by the powder can be increased for the improved efficiency of the energy source. Speed and efficiency are the primary reasons for the lower operating cost of EBM compared to LPBF. Moreover, higher temperatures during the production process imply lower thermal stresses in the parts and the possibility to produce components made of refractory materials. However, the material availability is limited by the conductivity of the metal and this technology is mainly applied for the production of parts made of Ti alloys, Co-Cr alloys and Inconel.

To avoid impurities and oxidation of the powder bed, the volume chamber is vacuumed before the start of production. Furthermore, the smoke effect due to partially charged particles need to be limited by partial sintering of the entire powder bed which also allows

the reduction of support structures. Nonetheless, after production, the parts need to be blasted to remove the partially sintered powder.

The resolution and the surface finish of parts produced with EBM is lower than the laser-based technique because of the possibility to reduce the laser spot dimension to a diameter approximately $75\ \mu\text{m}$ compared to the minimum diameter of an electron beam spot that is approximately $200\ \mu\text{m}$ [8].

1.2.3. DED

As depicted in Figure 3, in Directed Energy Deposition the part is fabricated by directly melting and depositing the metal from a wire or powder feedstock, therefore this technique doesn't require any powder bed. A multi-axes deposition head is used to feed the raw material through a nozzle and, simultaneously, to melt it with a heat source. The power source can be either a laser beam, an electron beam or a plasma arc [9]. As in the case of powder-bed based technologies, the laser beam requires an inert atmosphere, that can be also achieved with gas shielding, whereas the electron beam requires the build volume to be vacuumed to avoid the interaction between the electrons and the air.

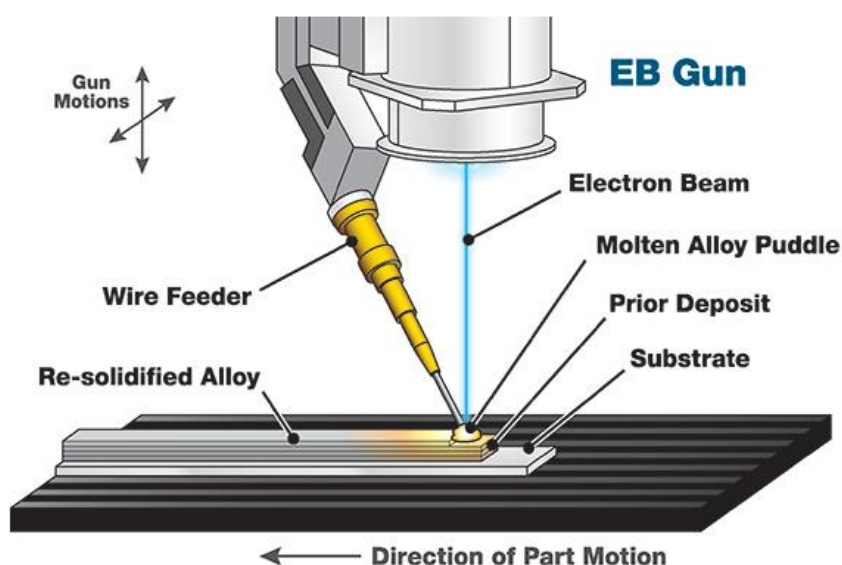


Figure 3. Schematic of a DED machine with electron beam power source.²

² Image from: <https://www.sciaky.com/additive-manufacturing/what-is-ded-3d-printing>

A unique feature of this technology is the possibility of using a preexisting component as a substrate to repair the part or coat a specific surface to improve mechanical and chemical properties. This is possible with the combined movement of the deposition head and the build platform avoiding the need for support structures. Moreover, the absence of a powder bed permits the utilization of generously sized build volume.

Despite the potential of DED as a multifunctional technology, it presents many criticalities: the low resolution often makes a post treatment necessary to achieve better surface quality and the big build volume implies the utilization of a great volume of inert gas for laser-based machines or a high-power vacuum pump for electron beam based machines. The utilization of gas shielding is effective in reducing the gas utilization, however excess powder would oxidize preventing recycling. To avoid oxidation of the powder a wire DED machine can be used, nonetheless the process parameters tuning is more critical in this case and the resolution of the part is poor making mandatory a further machining step. Last but not least, the creation of a melt pool has intrinsic drawback in terms of thermal stresses and distortion that can generate geometric defects in the part.

1.2.4. ADAM and BMD

In the case of the ADAM and BMD, similarly to what happens in the conventional polymeric *Fused Deposition Modelling* (FDM), the shape is given to the part through the extrusion of a filament of metal powder encased in a thermoplastic binder. The 3D geometry is achieved layer by layer by moving the extrusion head in a Cartesian Structure and the printing step is concluded with the creation of the so-called green body that is therefore made of both a polymeric and a metallic material. For this reason, it is necessary to debind the green part in a washing machine (at this stage the component is commonly referred to as the brown body) and then to sinter the powder and reach a solid component. The washing step is performed thermally in the case of ADAM and chemically in the case of BMD [10].

In Figure 4, the main components of the typical Cartesian structure of an FDM machine are depicted. As shown in the image, the ADAM and the BMD technologies feature a different spool for the support material to reduce and facilitate the post processing effort.

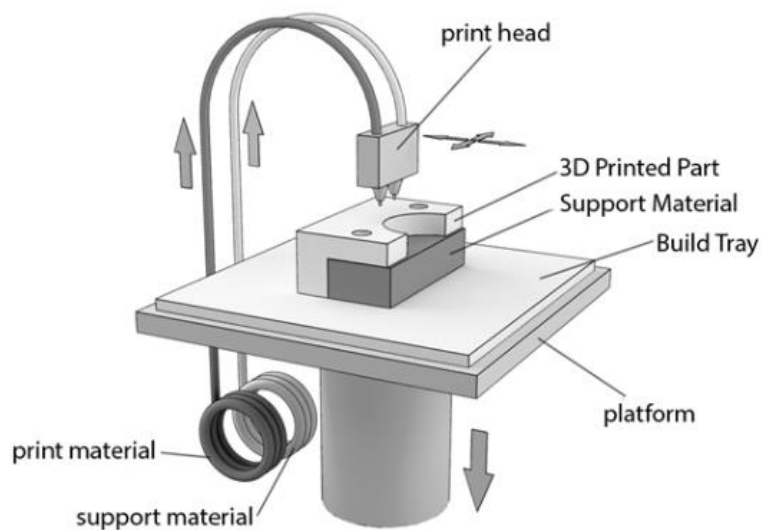


Figure 4. Schematic of an FDM machine ³

1.2.5. Metal Jet

The Metal Jet belongs to the *Binder Jetting* (BJ) AM techniques and it is based on the concept of binding the powder particles with a liquid binder. HP developed this idea to exploit the knowhow and the experience collected in the field of inkjet printers. Similarly to PBF techniques, also the Metal Jet machine presents a build box in which a layer of powder of given thickness is spread by a recoater. After the recoating, a crossbar on which printheads are mounted slides on the powder jetting the curing agent on demand and cures it directly with a heat source [11]. In this way, HP ensures to reach much higher printing speed with respect to the L-PBF technology and the print speed is just related to the part height and not to its volume. Moreover, since the sintering is performed afterwards in a furnace, the final part exhibits a more isotropic microstructure. However, having a powder bed, MJ also has the restriction related to the enclosed cavity for the powder removal.

³ Image form: <https://www.printie3d.com/learn-more-about-3d-printing/>

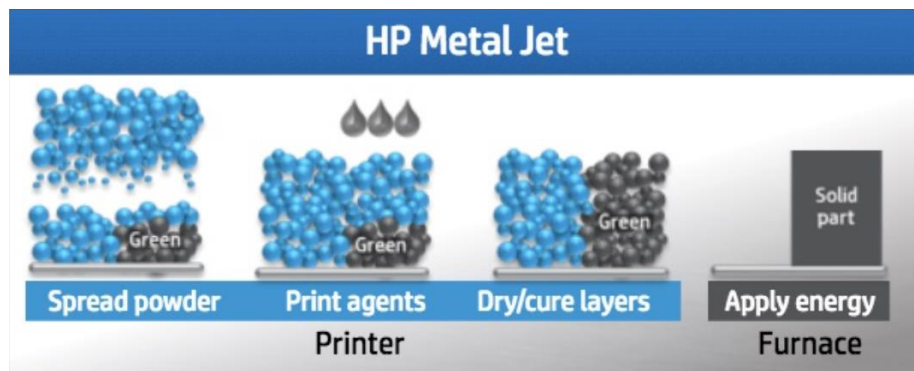


Figure 5. HP Metal Jet working principle [11]

In all cases, the indirect AM techniques require a further step with respect to the direct processes to debind the powder. During the debinding and the sintering steps shrinkage occurs in the part and this must be taken into account during the design of the CAD model by applying a proper scaling factor.

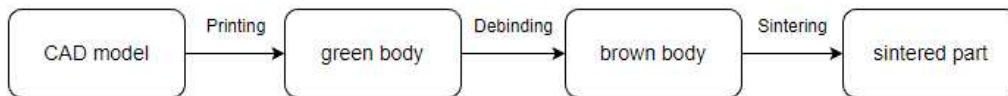


Figure 6. Workflow of indirect AM techniques.

2.State of the art

A brief introduction to the historical and technological background is given in this chapter to better describe the findings of the work. The technology investigated is based on a *Vat Photopolymerization* (VPP) AM technique, the *Stereolithography*, in which a photo-hardening resin is selectively cured layer by layer by a UV light to generate the desired 3D geometry for the final part.

2.1. Stereolithography

The first concept of additive manufacturing was developed in 1981 by Dr. Hideo Kodama [12]. The objective of his work was that of giving fine information about three-dimensional shape of an object useful in geometrical analysis and not that of producing functional prototypes. The technology was based on the idea of stacking cross-sectional layers of hardened resin to achieve the final geometry. The photo-hardening polymer was a mixture of unsaturated polyester, cross linking agent such as acrylic ester and styrene monomer, polymerization initiator, and sensitizer and it was curable with the exposure to waves with wavelength of about 300-400 nm.

As shown in Figure 7, three different setups have been tested by Dr Kodama: in (a), the light source was placed on top of the machine and a movable plate, on which the solid model was generated, was set in the liquid polymer. This plate was immersed intermittently by a pulsed motor together with the solidified layers. In (b), the light source was placed on the bottom of the tank and the movable plate was pulled up instead of being immersed. In (c), the liquid surface was exposed to UV rays through a scanning fibre transmitter. The fibre was mounted on a Cartesian XY plotter and the scanning speed, line width, and the area to be scanned were controlled by the machine. As a light source, a mercury lamp (200 W) or a xenon lamp (500 W) were used in (a) and (b). Both layouts (a) and (b) have been taken as a reference in the following years by manufacturer because of their different approaches that led to substantial difference in the usage of the resin.

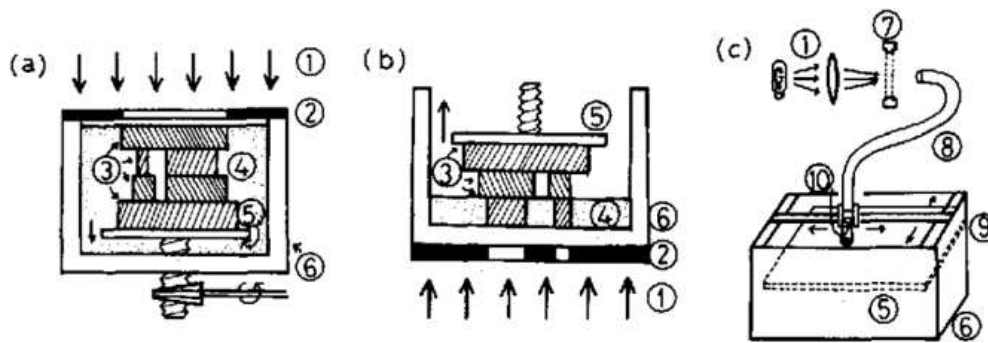


Figure 7. Different setup of H. Kodama SL machines

- ① UV rays, ② mask, ③ solidified layers, ④ liquid polymer, ⑤ movable plate, ⑥ tank, ⑦ shutter, ⑧ optical fiber, ⑨ XY plotter and ⑩ optical lens.

A few years after H. Kodama's publication, in 1986, Charles W. Hull patented the first SLA printer introduced in the market [13]. This time, the objective of the inventor was that of reducing time and costs of prototypes with respect to conventional manufacturing processes of polymers. As a matter of fact, injection moulding, that was the most common production technique, required high expenses for the tool design and fabrication both in terms of money and time. Moreover, the new technology allowed the integration of lithographic techniques to the informatic technology, to simultaneously execute computer aided design (CAD) and computer aided manufacturing (CAM) in producing three-dimensional objects directly from computer instructions.

As already seen in the work of H. Kodama, considering the position of the energy source with respect to the vat, two main categories of SL apparatus can be recognised: the free surface layout and the constrained surface layout [14].

2.2. Free and constrained surface layout

In the free surface approach (Figure 8, a), the energy source is placed on top of the vat and the build platform is positioned at a distance equal to the first layer height from the liquid resin surface. The UV rays cure the first layer that attaches to the platform and the platform is then lowered of a distance equal to the second layer height. At this point, a mechanical sweeper spreads the resin evenly on the platform and the light source cures the second layer that firmly attaches to the previous one. This procedure is repeated until the part is completed.

In the constrained approach (Figure 8, b), instead, the platform is suspended above the tank and it is immersed in the resin at a distance from the floor equal to the first layer height. The light is emitted from below the vat and it is transmitted through the transparent floor to cure the layer of resin between the floor itself and the platform. This cured layer attaches both to the platform and to the floor, therefore, a tilt movement of the tank is needed to detach the part from the tank and allow the vertical motion of the platform. When the platform reaches the defined distance to cure the second layer, the tank rotates back to its original position and the process is repeated. Since with this approach the part is printed upside down, it is also referred to as the “bat” configuration.

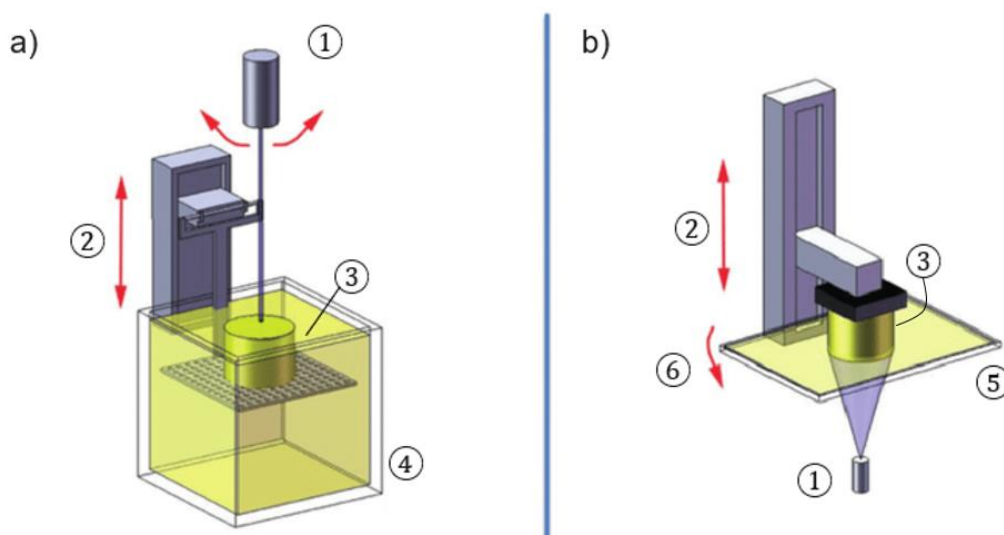


Figure 8. Free (a) and constrained (b) surface layout for SLA adapted from [15]

- ① light source, ② z-axis for the platform, ③ print attached to the platform,
- ④ vat containing liquid polymer, ⑤ transparent floor of the vat, ⑥ tilt motion of the vat

Between the two approaches, the most adopted is the bottom-exposure one since it can avoid the necessity of soaking the part in the liquid resin reducing the printing costs and making the part height not limited by the vat height. Moreover, a better control of the layer thickness is achieved by adjusting the z level of the platform and the mechanical sweeper is removed. Last but not least, this configuration prevents the interaction of the resin with the air oxygen that negatively affects the curing dynamics. On the other hand, “bat” configuration printers must adopt some strategies to counteract the adhesion of the part to the vat floor. To handle this issue, a tilt motion is implemented to the tank with a

motor. Some other solutions have been developed to reduce the floor-part interaction such as the application of hydrophobic coatings or shear forces [14, 15].

Another classification of the SLA machines can be done on the basis of the typology of light source and on the manner in which the light is shaped to cure the layer of resin.

2.3. Irradiation techniques for SLA

During the last four decades, a great variety of technologies have been applied to SLA. Between them, the most common are the Laser-SLA and the *Digital Light Processing SLA* (DLP-SLA) whereas the *Masked SLA* (MSLA) are usually low-price printers for hobby and semi-professional users. Moreover, some more advanced techniques have been implemented to rather increase the resolution or the printing speed or both [14].

2.3.1. Laser-SLA

Laser-SLA, also known simply as SLA, is the technology in which the liquid precursor in the vat is selectively cured by a laser. The laser scans the sectional view of the object with the use of a dual axis galvo system endowed with mirrors that enable a rapid and accurate XY motion of the laser spot. Dedicated scanning strategies are necessary to optimize the resolution and minimize printing time, shrinking and warping issues related to the curing of the resin [16, 17]. In Figure 9 the main components of a constrained-surface laser-SLA printer are shown:

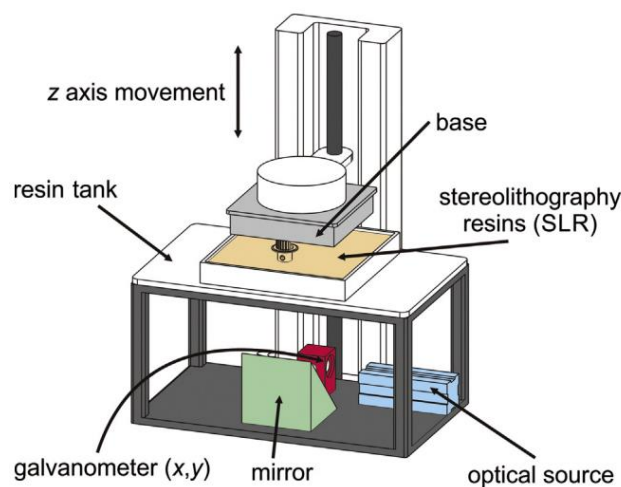


Figure 9. Laser-SLA setup [18]

The main parameters affecting the resolution and printing speed are scanning speed and diameter of the laser spot and the layer height. By tuning these parameters, a resolution of 5-10 μm can be achieved [14].

Starting from the laser-SLA, other techniques have been developed to achieve finer resolution. Among these it is worth to mention the *Two Photon Polymerization* (TPP) that has been proved to achieve a resolution of about 100 nm [19]. Furthermore, other concepts exist such as the *pinpoint solidification* that was born with the intent of increasing resolution without introducing the pulsed laser as in the TPP and the *bulk lithography* in which speed and power of the laser are adjusted to generate a 3D object with a non-layered approach [14].

2.3.2. Masked-SLA

Even though the fabrication of prototypes can be accomplished in a faster way compared to conventional manufacturing processes, the Laser-SLA approach, in which each component is generated layer-by-layer in a sequential manner, limits the throughput for mass production. To increase the productivity, the so called Masked-SLA has been invented. The idea is to mask the light projected by the light source with the shape of the cross section of the part in order to cure simultaneously the layer. This concept is used to decouple the dimensions of the section of the printed object from the printing time, that is only related to the height, and increases the benefits in fabricating multiple components in a single print. The usual choice for the light source is a UV-LED matrix, whereas a *Liquid Crystal Display* (LCD) is commonly used as mask and it is interposed between the vat floor and the light source (considering a bottom-exposure setup) as shown in Figure 10.

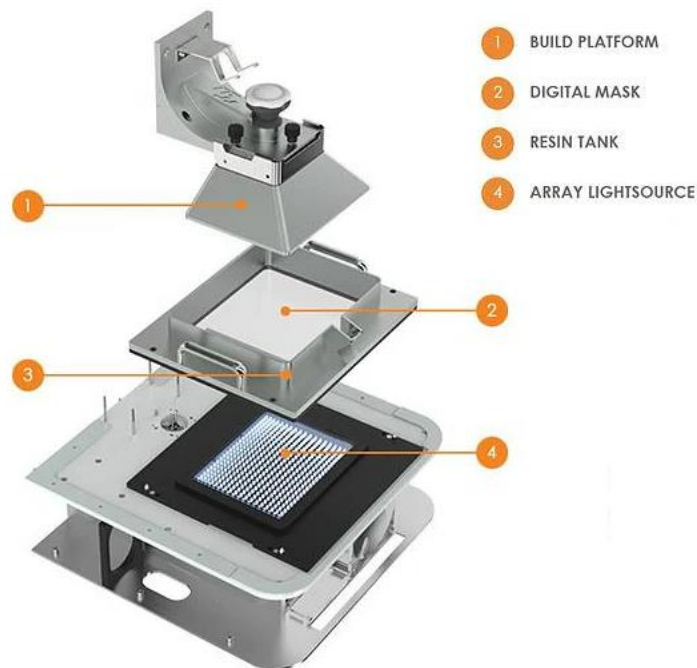


Figure 10. Components of a MSLA printer ⁴

Activating or deactivating the LCD pixels, the light is transmitted or not to the vat floor and then to the resin. This working principle implies a direct relationship between the resolution of the LCD and the resolution of the part. In terms of detail quality, with respect to the SLA, MSLA cures the part in a discrete manner where the smallest entity is the *voxel* (from the union of volume and pixel) and the lateral resolution is in the range of few tens of microns for commercial printers [20]. This means that LCD SLA is excellent for curing sharp edges but can cause saw-tooth type surface roughness on curved surfaces.

2.3.3. DLP-SLA

Despite the capability of reaching high throughput, the LCD technique has some intrinsic criticalities that limit the effectiveness of this solution. First of all, as described in 2.3.2, the resolution is limited by the pixel dimension, but this is not the only drawback: a portion of the light transmitted through a pixel is absorbed even during the ON mode and the switching speed is in the quite low (~ 20 ms) [21]. Moreover, some light bleeding

⁴ Image from: structo3d.com

during the OFF mode is possible [22]. To overcome these problems, DLP technology has been applied to SLA.

The fundamental component of DLP-SLA is the *Digital Micromirror Device* (DMD) that acts as a dynamic mask. It is made of a matrix of micro-mirrors that are electronically individually controlled and it is used to reflect the light emitted from the light source in the desired shape. The energy source is again a UV-LED and the light, after reflecting on the micromirrors, is transferred through a reduction lens to the resin surface. The reduction lens is used to reduce the feature size on the printed part with respect to the projected image from the DMD. As in MSLA, also with this technology the entire layer is cured simultaneously, keeping high production speed levels. A comparison between DLP and LCD technologies is given in Figure 11:

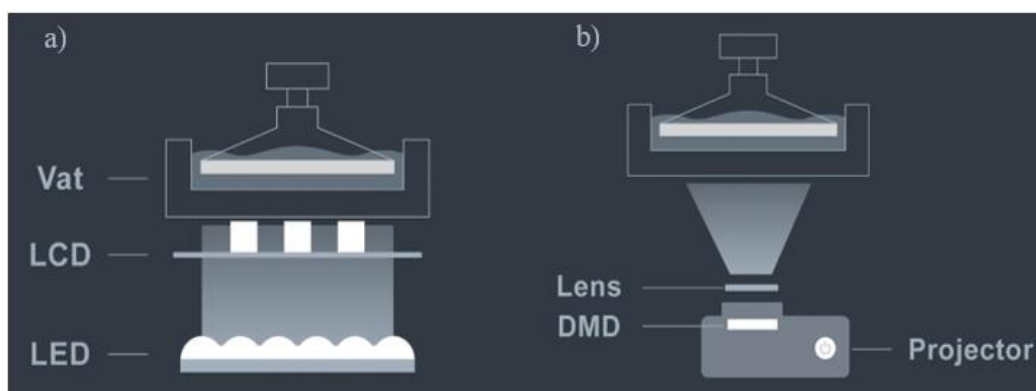


Figure 11. Comparison between LCD (a) and DLP (b) ⁵

The flexibility given by the DMD can be used to increase or reduce the projected image scale. This means that the total amount of pixel can be distributed on a wider or smaller print surface making the resolution inversely proportional to the print area of the object. This capability is fundamental to reach accurate print for small object but may lead to lower accuracy for large print surfaces. Another advantage over LCD is that DLP is claimed to be more resistant and suffer less wearing issues making this technology more suitable for industrial applications. However, also DLP has some criticalities mainly related to the distortion of the image due to the different dimensions of the DMD and the printing area. This effect is more visible on large prints since it is proportional to the

⁵ Image redesigned from: phrozen3d.com

distance from the centre of the printing area; nonetheless, a software adjustment can be introduced to reduce the distortion [22].

Based on the fast switching capabilities of the micromirrors in DLP, a new technology has been developed by Carbon Inc. in which the part is printed in a continuous manner avoiding the slicing procedure. This technology is called *Continuous Liquid Interface Production* (CLIP) and it features an oxygen permeable film that prevents local curing of the resin at the vat floor allowing continuous flow of the uncured resin below the polymerized one. The light is projected without interruption (similarly to what happens in a common video) and the platform is moved continuously in the Z direction in order to complete the print in a unique step reaching the highest throughput available for SLA nowadays. Moreover, the stepped appearance typical of layered manufacturing is avoided [23].

2.4. Resin for SLA

Resin for SLA must present some specific characteristics to enhance the production speed, efficiency, reliability and quality and to ensure good mechanical properties of the hardened component. Obviously, also the health of the operator must be taken into account during the entire process duration, meaning both when the resin is liquid and when it turns solid. Thus, a good resin for SLA must show:

- High reactivity to UV light
- Low activation energy
- Low viscosity
- Low shrinkage
- Reduced sensitivity to atmospheric agents (e.g., moisture and oxygen)
- Good mechanical properties after polymerization
- Low volatility and toxicity.

To achieve the desired characteristics, resin producers can work with different constituents both in terms of typology and quantity. The primary elements that characterize the resin are the *precursors* and the *Photoinitiator* (PI). As shown in Figure

12, some *additives, fillers and UV absorbers* can be added to the composition to modify the chemical and physical properties of the resin before and after curing.

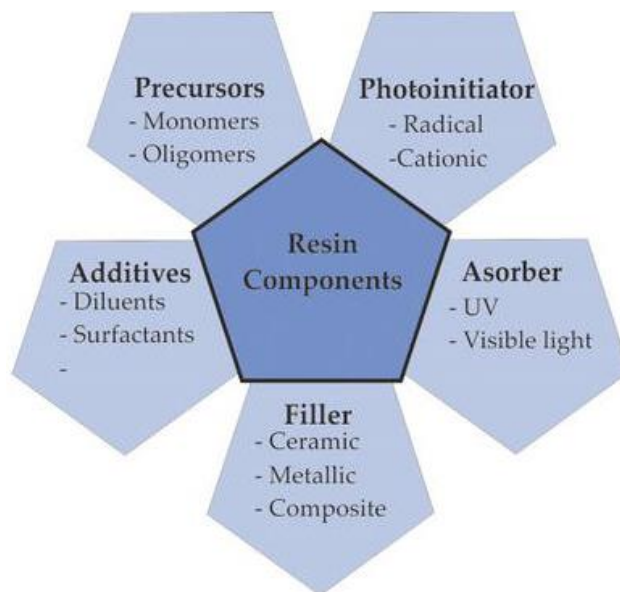


Figure 12. Resin for SLA [14]

It is worth mentioning that the resin for SLA are thermosetting materials, therefore they are not recyclable. This aspect is crucial because, in VPP processes, support structures are made of the same material of the green part and there is no possibility to recover them. To reduce the environmental impact, some biodegradable photopolymer resins have been developed and applied in stereolithography printing [24].

2.4.1. Precursors

The precursors are the monomers and oligomers that crosslink to create a solid structure after the polymerization. The monomers provide viscosity control, as well as impart properties based on their structure. Highly functional monomers (containing at least two double bonds) increase crosslink density of the polymer, increasing in this way hardness of the hardened polymer. The oligomers, instead, impart properties associated with their basic structure [25]. These are the main constituent of the resin and define the family of the resin itself differentiating the acrylic from the epoxy.

Acrylic resins, mainly made of acrylate monomers ($\text{CH}_2=\text{CHCO}_2\text{R}$), have a curing kinetics based on radical polymerization and exhibits high reaction speed that is crucial

for reaching high throughput. Despite their rapid curing and good spatial resolution, acrylate systems commonly show low toughness and tend to be brittle because of their high cross-link density and inhomogeneous architecture [24]. Moreover, this kind of resins are affected by a significant shrinkage during curing and the polymerization is limited by the oxygen present in the air. To limit shrinkage, a blend with epoxy resin or the combination with methacrylate is used whereas mechanical and physical properties can be tuned by changing the number of functional groups or with the addition of oligomers [14]. Also, the ratio between oligomer and monomer in a resin have an effect on the polymerization curve: experimental test conducted by E. Andrzejewska and M. Andrzejewski have shown that, for an acrylic resin, the fastest polymerization is reached with an equimolar mixture of monomers and oligomers [25].

Epoxy systems, based on the cyclic ether epoxide ($R-O-R'$), have a polymerization of the cationic type and need longer reaction times, are inhibited by moisture, but have the advantage of stability against oxygen and show lower shrinkage with respect to the acrylic resin. As mentioned above, a blend of the two family is commonly used in commercial resins to achieve the best compromise in terms of curing speed, shrinkage and mechanical properties [14].

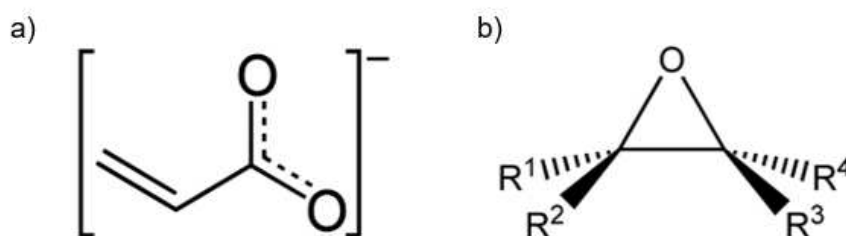


Figure 13. Acrylate ion (a) and epoxyde cyclic ether (b)

2.4.2. Photoinitiator

The photoinitiator is the moiety of the resin that reacts to light and initiate the curing process both in the case of cationic and radical polymerization. The PI type and concentration has a direct effect on curing speed, through cure, cross links density, hardness and other mechanical properties of the printed part [14, 26].

Since the formation of reactive species by direct light absorption of monomers is not effective in short times, the initiation step of the polymerization reaction requires the presence of a PI capable of generating these reactive species. Once the reactive species react with the monomers, the chain propagation can happen. To extend the light sensitivity to a broader range of wavelength, a light absorber (or photosensitizer) can be added to the resin. This molecule is able to absorb the light energy and to excite the reaction of the PI [26].

2.4.3. Fillers

Production of ceramic components is possible with SLA in an indirect process by filling the resin with fine ceramic powder. As in the other indirect techniques discussed in paragraph 1.2., also in this case the production is ended with the creation of the green part that has then to be debinded and sintered. Obviously, the particle size must be smaller than the layer height [14]. Some attempt in printing metal parts have also been done by P.J. Bartolo and J. Gaspar [27]. The effects of fillers on resin rheology and curing kinetics are analysed in the following chapter about filled resin.

To improve sedimentation stability and resin flowability, additives such as dispersant can be incorporated in the polymer. The choice of the proper additive and its concentration are crucial to reach a high filling ratio and to make long printing times possible.

2.5. Filled resin for SLA

As already described in the previous section, ceramic filled resins are commonly used to produce ceramic components with stereolithography whereas metal filled resin are not as researched. The introduction of a powdered filler, however, makes critical several aspects related to resin rheology and suspension stability, to air incorporation and to the curing kinetics since the particles greatly interact with the light. The rheology of the compound and the air incorporation can be addressed by using proper dispersing and defoaming additives and by vacuuming the mixture; for the particles-light interaction, instead, the optimal composition base resin composition should be found to achieve a satisfactory curing behaviour.

2.5.1. Scattering of light

In [28], the minimum ceramic load to produce reliable, dense finished parts, is estimated to be the 50 vol% of the resin. Moreover, the viscosity of the resin is limited to 5 Pa·s to avoid problems in the recoating step during the printing process. At this filling ratio, scattering has a detrimental effect on the depth of penetration of the light and causes a widening of the printed surface. S. Bhattacharjee explains that the effect of spreading the radiation sideways is related to the particles dimension in proportion to the wavelength λ of the radiation [29]. In the same reference, Rayleigh scattering for small particles ($d < \lambda/10$), and Mie scattering for relatively large particles ($d \geq \lambda/10$) are described. As illustrated in Figure 14, Rayleigh scattering considers a uniform, elastic scattering (without loss of energy) whereas Mie scattering is inelastic and angle dependent.

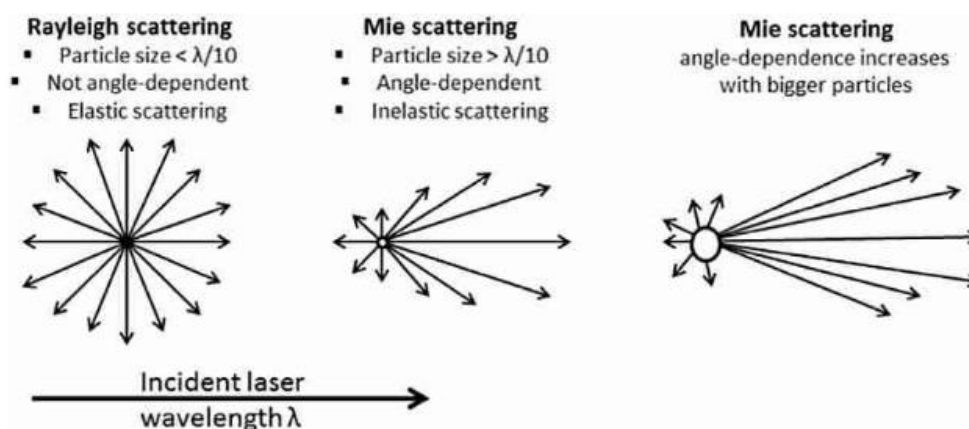


Figure 14. Rayleigh and Mie scattering [29]

Since in SLA technology, the lightsource chosen to polymerize the resins has a wavelength of about 400nm, and the particles dimension ranges between few tenths of a micrometer to some tens of micrometers, our application falls in the Mie scattering regime. This means that the scattering should be more intense towards the direction of the incident light rather than sideways, and this anisotropy is more evident with larger particles. Nonetheless, the side polymerization must be taken into consideration during the setting of the print parameters. In [28], the following equation has been used to describe the effect of scattering on cure depth:

$$C_d = \left(\frac{2}{3} \cdot \frac{d}{\Phi \beta \Delta n^2} \right) \ln \left(\frac{E}{E_c} \right) \quad \text{Eq 1}$$

where C_d the curing depth, d the median particle size, Φ the volume fraction solids, β a term that involves interparticle spacing and wavelength of radiation and Δn is the difference in index of refraction between the suspended particles and medium (resin). Moreover, E and E_c are the average exposure dose supplied by the energy source and the critical exposure of the resin. Eq 1 highlights the fact that the curing depth is proportional to the mean particle size and inversely proportional to the volume fraction of the powder. Furthermore, a detrimental effect on curing depth may be given from the light absorption of dark particles that act as grey body.

2.5.2. Dispersants

Dispersants are used to reach a stable suspension of particles in the resin, reducing phenomena related to flocculation and settlement.

Flocculation is caused by the attractive London-van der Waal forces occurring between the particles. These forces are effective only across a small distance; however, they cause the particles to collide or at least to become too close to each other and therefore creates flocculation. It follows that, to stabilize a system against flocculation, the establishment of repelling forces between the particles is required. An effective representation of the interaction between the attracting and repelling energies is the plot of the potential curves as a function of the distance between particles [30]. As shown in Figure 15, the summation of both curves results in the total energy, which represents the amount of thermal energy that a particle must have to agglomerate, i.e., it is an index of the deflocculating power of the dispersant.

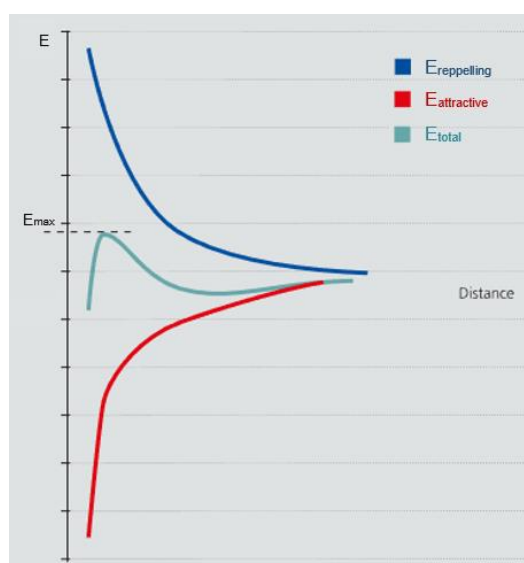


Figure 15. Potential curves of particles attraction and repulsion [30]

The stabilizing effect of dispersant is achieved with the combination of electrostatic repulsion and steric stabilization.

Electrostatic stabilization is based on the concept of the *electrical double layer* that consists in the formation of an adsorptive bound layer and a diffuse layer on the particle surface. The first layer consists of ions adsorbed onto the object due to chemical interactions; the second, instead, is made of free ions that move in the fluid under the influence of electric attraction and thermal motion. Dispersing additives can be used to influence the surface charge of the particle favoring strong charges that are used to generate high repulsion potential and thereby suppresses flocculation.

In steric stabilization, instead of generating electrostatic forces, the repulsion potential is produced by the absorption of the polymer on the particle surface and the subsequent generation of an envelope of dispersant molecules around the solid. When two particles get close, they overlap and penetrate these envelopes increasing the polymer concentration in the overlapping area. At this point, the osmotic pressure causes the solvent to be transported to this area so that the particles are repelled away from each other again. Moreover, due to the interaction of two approaching particles, the polymer molecules are restricted in their conformation, which means a reduction in the entropy and therefore represents a repulsion potential [30].

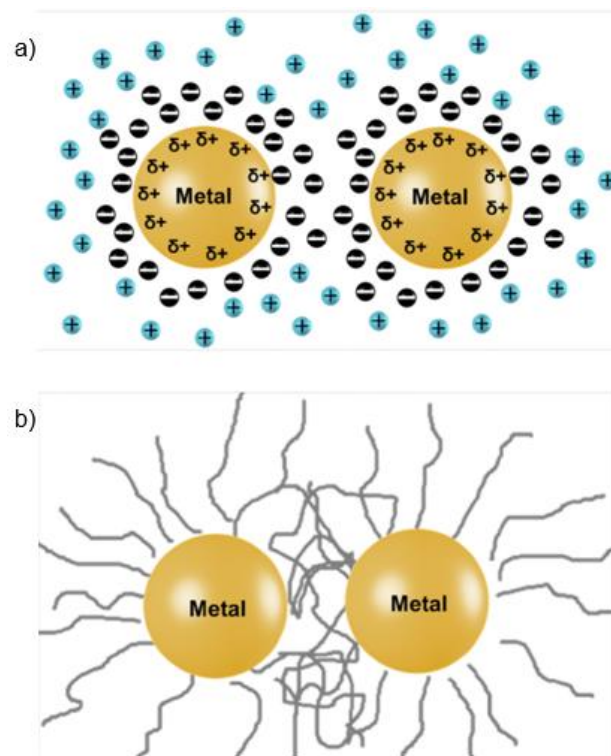


Figure 16. Electric stabilization (a) and steric stabilization (b) [31]

3. Experimental implementation

The experimental procedure of this work is thought to define a resin composition that allow a fast and deep curing, high suspension stability and low viscosity in order to produce a defect-free metal component in an indirect LCD-SLA process.

First of all, the characterization of the used powders and the analysis of the effect of their embedding in the resin was performed. After that, the focus moved toward the optimization of the resin composition in order to achieve suitable curing depth and curing speed and to reduce settlement phenomena. Once the resin was stabilized, the printing parameters have been optimized for our system to reach full solid green bodies. Subsequently, some brown bodies have been produced.

3.1. The printer

Before starting with the experimental description of the project, it is useful to state the characteristics of the available stereolithography apparatus. The printer is a Prusa SL1S, an MSLA with a constrained surface layout. The light source is a matrix LED emitting rays with wavelength $\lambda = 405$ nm and it is masked by a 5.96" LCD screen with a resolution of 2560x1620 pixels. The maximum building volume is 127x80x150 mm and the minimum layer height is 0.01 mm. These characteristics are expected to satisfy the requirements for this work in terms of resolution and layer height.



Figure 17. Prusa SL1S printer

3.2. Analysis of the powders

The analysis of the powders was divided in two steps: firstly, the *Particle Size Distribution* (PSD) was measured with a laser diffraction particle size analyzer (Figure 18) and subsequently an examination of the powder at the microscope was used to determine the powder morphology. It is worth noticing that, by default, the PSD was given in a volume distribution meaning that the bigger particles have more weight on the average than the smaller ones (i.e., the curve is shifted toward higher values with respect to the number PSD).



Figure 18. Laser diffraction particle size analyzer⁶

Two different microscopes have been utilized: a transmitted light microscope, and a scanning electron microscope (SEM). The former requires the incorporation of the particles in a liquid medium, which can be water-based or polymeric, to be spread on a slide and then analyzed. The latter, instead, can be directly used to examine samples of dry particles.

3.3. Critical aspects for resin printability

As already explained in the paragraph 2.5 about filled resin, the main aspects to consider for resin printability are related to suspension stability and curing kinetics.

⁶ Mastersizer 3000 from Malvern Panalytical

3.3.1. Suspension stability

The suspension stability has been tested in a rheometer (Figure 19) able to extract the values of *storage and loss moduli* (G' and G'' respectively) as a function of oscillations of variable amplitudes and different frequencies. Moreover, the same machine was used for the analysis of the resin viscosity. The experiments were conducted with a parallel plate configuration and a closed-loop control on the temperature with a dedicated liquid cooling circuit.



Figure 19. Rheometer with parallel plate configuration⁷

G' , G'' and viscosity values are useful to compare the effectiveness of different dispersants and the eventual synergies with increasing powder concentration. Entering more in detail, our attention was reserved to the difference between the values of storage and loss moduli in the range of low shear and low frequencies, i.e., the conditions encountered during the printing phase. A G' value similar to or greater than the G'' value is an indicator of a good stability of the resin and the higher the difference, the more pronounced is the solid-like behavior of the resin.

⁷ MCR 302 from Anton Paar

3.3.2. Powder-light interaction

The interaction between particle and light is mainly related to the volume fraction, the dimension of the particles and the filler material chosen. To analyze the effects of these three parameters on the curing speed and curing depth, the *Photo-Rheology* (PR) test is performed, and the samples are analyzed with the reflected light microscope.

The PR test is used to measure the value of G' of a sample of resin during the polymerization induced by an energy source. In our project, we performed these measurements with the integration of a UV light source into the same rheology machine used for rheological measurements. The system is adapted with an FDM 3D printed clamping unit designed to hold in position a glass slide on which the resin is deposited (Figure 20). The slide is used to allow the irradiation of the resin from the bottom, where the same LED matrix used in the printer is positioned (without the LCD screen). On top of the slide, the parallel-plate configuration of the rheology machine is used.

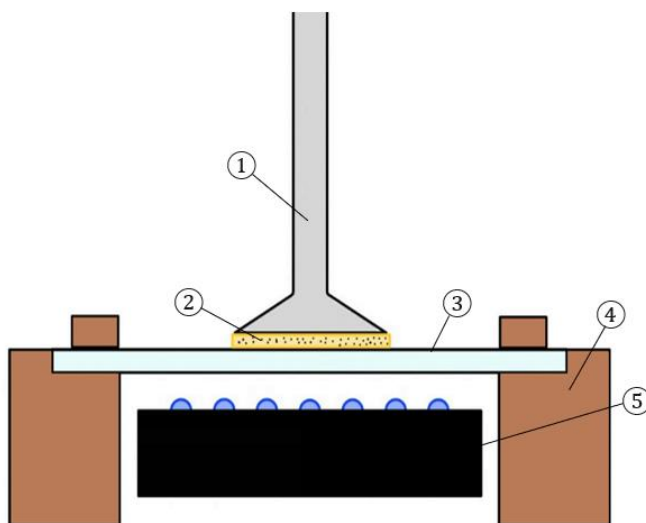


Figure 20. Photo-rheology setup

- ① rotating plate, ② filled resin, ③ glass slide, ④ clamping unit, ⑤ UV-LED matrix

This test is useful not only for the numerical results given by the machine, but it also produces small discs of cured resin that can be analyzed afterwards. As a matter of fact, in case of incomplete curing (when the cure depth is lower than the distance between the slide and the plate), the thickness of these samples is measured with a micrometer to have

a first evaluation of the curing depth. Furthermore, the discs can be embedded in epoxy resin, grinded and polished and then analyzed at the reflected light microscope. Here, an effective visualization of the suspension stability can be obtained, and the presence of air pockets can be detected. Moreover, incomplete curing can be visualized and measured with higher accuracy with respect to the use of the micrometer.

3.3.3. Air pockets

Air trapping can negatively influence the curing kinetic of the resin. This can be detected with a PR test. Air pocket effects on PR can indeed be reduced by vacuum mixing the resin right before the test. Another improvement can be achieved with the introduction of a defoamer in the resin composition that may even overcome the need of the utilization of a vacuum mixer. The cured samples produced by the PR test can then be embedded in epoxy resin, grinded and cured to analyze the air pockets at the reflected light microscope. To improve air pockets detection, a smartphone holder (Figure 21) has been designed and produced with an FDM machine. This tool allows for the recording of videos in which it is possible to see scans of entire samples and the investigation of air pockets is done by sliding the focus in and out.

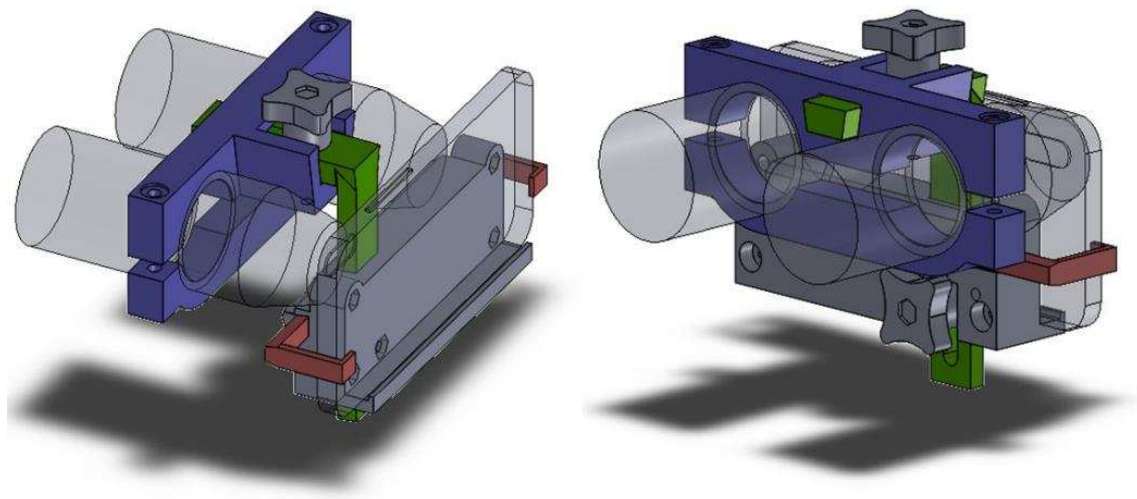


Figure 21. Smartphone holder for microscope videorecording

3.4. Printing parameters

Due to the higher viscosity, the slower curing kinetic and the lower curing depth, printing parameters of filled resin are quite different from the ones of the base resin. These parameters can be easily modified in the slicing software and therefore they are not related to the CAD model drawing.

3.4.1. Exposure time of the first layer

The exposure time of the first layer is the amount of time dedicated to the irradiation of the first layer. This parameter is crucial to enhance the adhesion of the first layer to the platform. On the other hand, over-exposure may lead to side curing and loss of detail due to scattering of light. Moreover, increasing the time of exposure of the first layer, also the total printing time is increased. Introducing a pad below the object (Figure 22) to be printed can overcome the issue of over-exposure, however it will increase the scrap⁸ and the printing time.

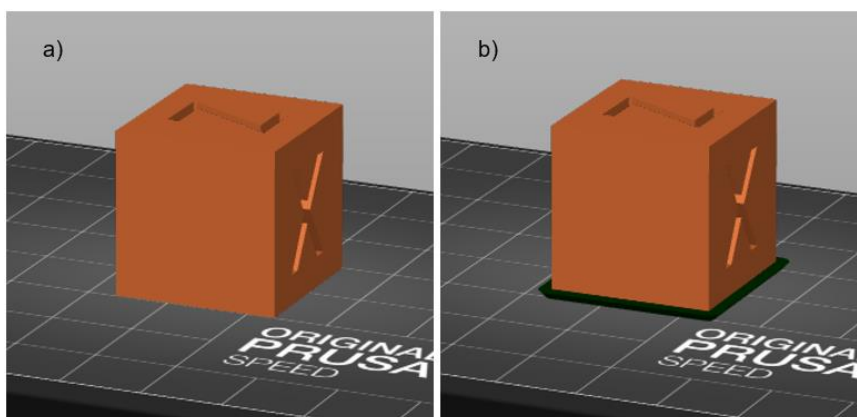


Figure 22. Example of a component without pad (a) and with pad (b)

⁸ Since the resin is a thermosetting material, scraps cannot be recycled.

3.4.2. Exposure time

The exposure time is the time of irradiation of all the layers from a defined one until the end of the print. The transition between the first layer exposure time and the final exposure time happens by reducing the values in a defined number of layers called “faded layers”. The exposure reduction doesn’t follow a linear trend and the algorithm implemented in the software is proprietary, therefore the only tunable parameters are the number of faded layers and the final exposure time.

As for the exposure time of the first layer, also this time is a compromise between layer adhesion, resolution and printing time. In this case, the adhesion is between 2 resin layers and not with the platform, therefore a lower amount of energy is required. The printing time is largely affected by this parameter, especially for tall components.

3.4.3. Layer height

Using filled resin, minimum layer height is constrained by the particle size distribution. A layer height lower than the particles’ dimension inside the resin is not feasible; on the other hand, an excessive height leads to poor resolution in z-axis and to weaker layer adhesion with the risk of incomplete print.

In terms of printing time, increasing the layer height has two contrasting effects: on one side it reduces the total number of layers, on the other side it makes necessary to also increase the exposure time for each layer to reach deeper curing. To enhance the adhesion to the platform, it is possible to adjust the height of the first layer separately by reducing the z-offset that is the distance of the platform to the FEP film of the vat.

3.4.4. Tilt time

Due to its high viscosity, the resin requires more time to flow and to cover the FEP film completely. For this reason, the time reserved for the tilting of the tank is increased. Obviously, increasing the tilt time also the printing time is increased proportionally.

3.5. Debinding and sintering

Debinding and sintering of aluminium powder requires a furnace with controlled atmosphere. Due to the high reactivity of aluminum with oxygen, the usage of a furnace without any control of the atmosphere leads to ineffective sintering; yet some tests on the effect of powder content on the shrinkage of the part after debinding can be performed.

4. Results and discussion

4.1. Powder characterization

In our analysis we have considered 5 different powders to understand how the filler can affect suspension stability and polymerization. The first powder is a recycled Al alloy with silicon and magnesium (AlSi10Mg) conventionally used for L-PBF techniques. This powder has been compared to an Al₂O₃ used for the production of ceramic components with SLA technology, to a 316L stainless steel powder and to the almost eutectic AlSi12 alloy powder. Moreover, since the AlSi10Mg powder was affected by a large number of defects due to the recycling process, a sieving operation has been performed with a vibrating sieving machine in the range between 20 μm and 36 μm.

4.1.1. Particle Size Distribution

The PSD of the aforementioned powders were analyzed with the laser diffraction particle size analyzer and the results are reported in Figure 23:

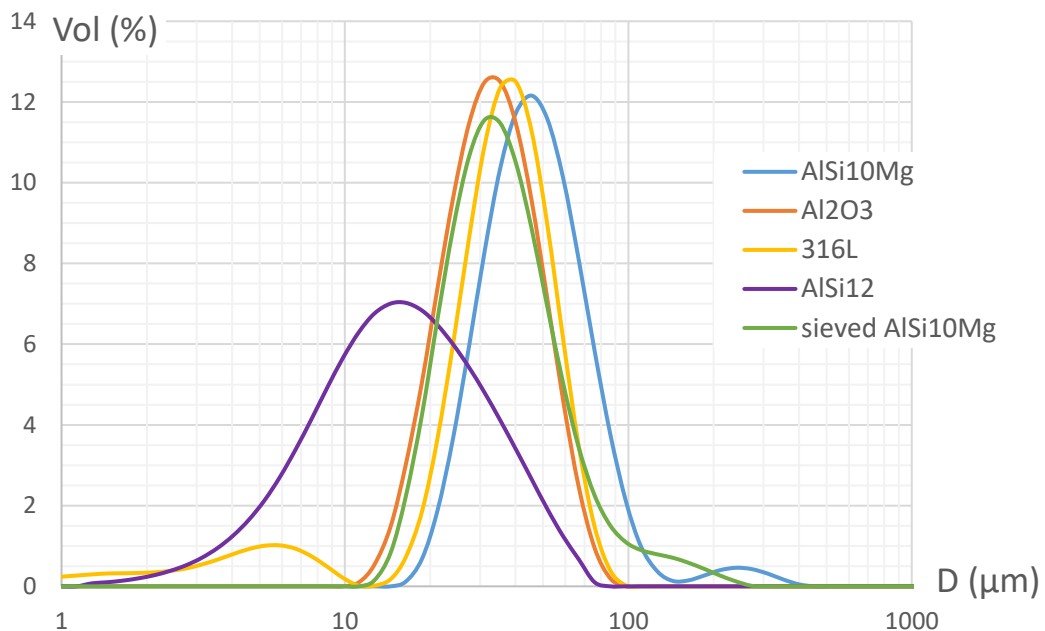


Figure 23. PSD of the used powder

As shown, the PSD of AlSi10Mg powder is slightly shifted toward the right with respect to all the others meaning that the average particle size is greater. After sieving, the mean particle size decreased to a value similar to the ones of the Al₂O₃ and the 316L powders; however, the right end of the curve still presents a non-symmetric tail presumably caused by some residual large particles from the recycling. The leftmost curve is related to the AlSi12 powder, which has particles in the range of a few micrometers. Nonetheless, this powder also presents a broader distribution with respect to the others with the curve that is dropping to the zero at a particle diameter greater than 50 μm.

The values of D10, D50 and D90, which correspond to the tenth, fiftieth and ninetieth percentile of the PSD respectively, are reported in Table 1 for each powder.

Table 1. Values of D10, D50 and D90 of the examined powders

Powder	D10	D50	D90
	μm	μm	μm
AlSi10Mg	29.62	49.26	85.56
Al ₂ O ₃	21.08	34.92	57.02
316L	7.60	37.78	60.70
AlSi12	6.38	16.62	40.14
sieved AlSi10Mg	19.43	40.65	67.76

The D90 can be considered as an indicator of the minimum layer height because above this value only 10% of particles by volume can be found.

4.1.2. Particle morphology

The particle morphology may influence the sedimentation phenomenon and the air trapping, thus a comparison between the powders is given in this paragraph.

The analysis of particle morphology of AlSi10Mg (Figure 24 and Figure 25) and Al₂O₃ (Figure 26) powders has been performed with the transmitted light microscope by suspending a small number of particles in an acrylic resin. The micrograph of 316L (Figure 27) and AlSi12 (Figure 28) powders, instead, are taken at the SEM and therefore, the powder has not been incorporated into the resin.

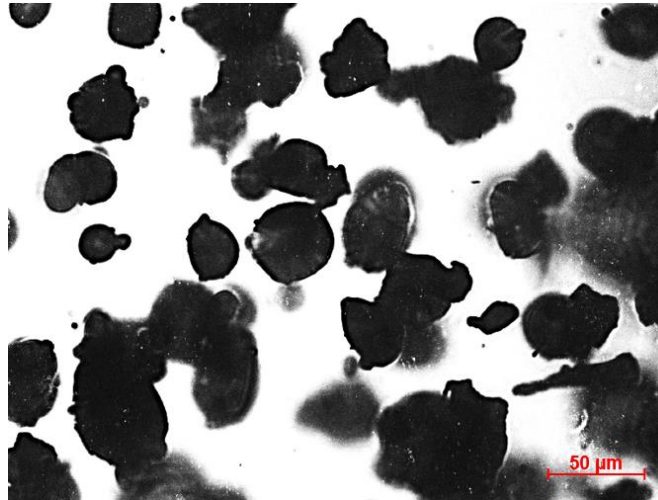


Figure 24. Micrograph of AlSi10Mg powder in acrylic resin

Figure 24 illustrates how the AlSi10Mg powder is mostly non-spherical and presents some agglomerates and elongated particles. Moreover, as already stated by the quite broad PSD curve (Figure 23), the size of the particles varies in a wide range.



Figure 25. Micrograph of sieved AlSi10Mg powder in acrylic resin

After sieving, the particle morphology seen in Figure 24 was preserved but the size of the particles was more homogeneous with a considerable reduction in average dimension. The imperfect sieving can depend on some defects in the sieve or in the alignment of the elongated particle with respect to the sieve's holes. However, this process was necessary to achieve the target PSD and to remove the impurities.

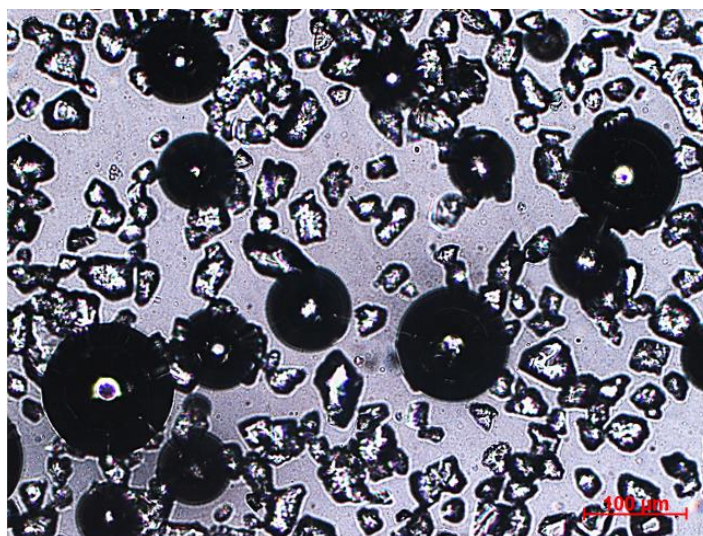


Figure 26. Micrograph of Al_2O_3 powder in acrylic resin

Figure 26 shows that the alumina powder is composed of non-spherical particles with sharp edges and rough surfaces and there is a good dimensional consistency of the particles that have a narrow size distribution. With respect to the aluminium powder, at the transmitted light microscope the ceramic particles appear to be brighter due to the difference in color that may influence the curing kinetics.

In the micrograph, the presence of air pockets was also noticeable. These are shown as dark perfect spheres with a bright region at the centre.

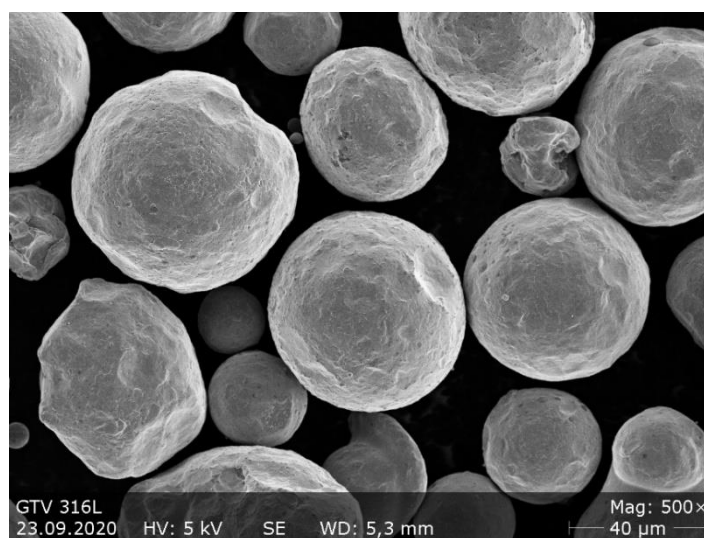


Figure 27. SEM micrograph of 316L powder

Figure 27 highlights that the steel powder presents almost spherical particles with few defects. Some surface roughness can also be detected.

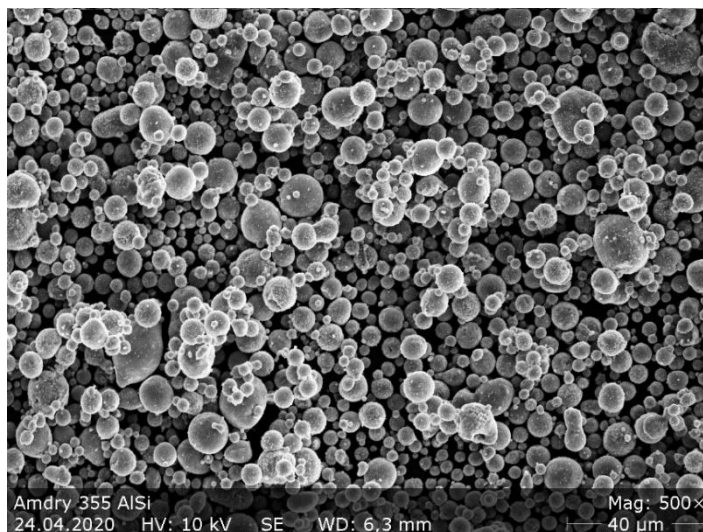


Figure 28. SEM micrograph of AlSi12 powder

Figure 28 shows the AlSi12 powder with mostly spherical particles but also some agglomerates and elongated particles. The broad range of particle dimension, which was highlighted by the laser diffraction particle size analyzer, is evident.

4.2. Curing kinetics

The effects of the filler on photo rheology can be analyzed with the PR test, measuring the curing depth and examining the cured samples at the reflected light microscope.

4.2.1. Effects of the filler on curing behavior

Starting with the evaluation of the effect of the filling ratio on the curing kinetics, a good indicator of polymerization speed and through cure is given by the slope of the PR curve and its final level of G' . Photo-rheology curves (Figure 29) show the trend of G' versus time during the polymerization; therefore, a steeper slope means that the polymerization is faster.

To perform these tests, the powder has been mixed with an acrylic resin in a planetary mixer right before the sampling to avoid settlement of the particles.

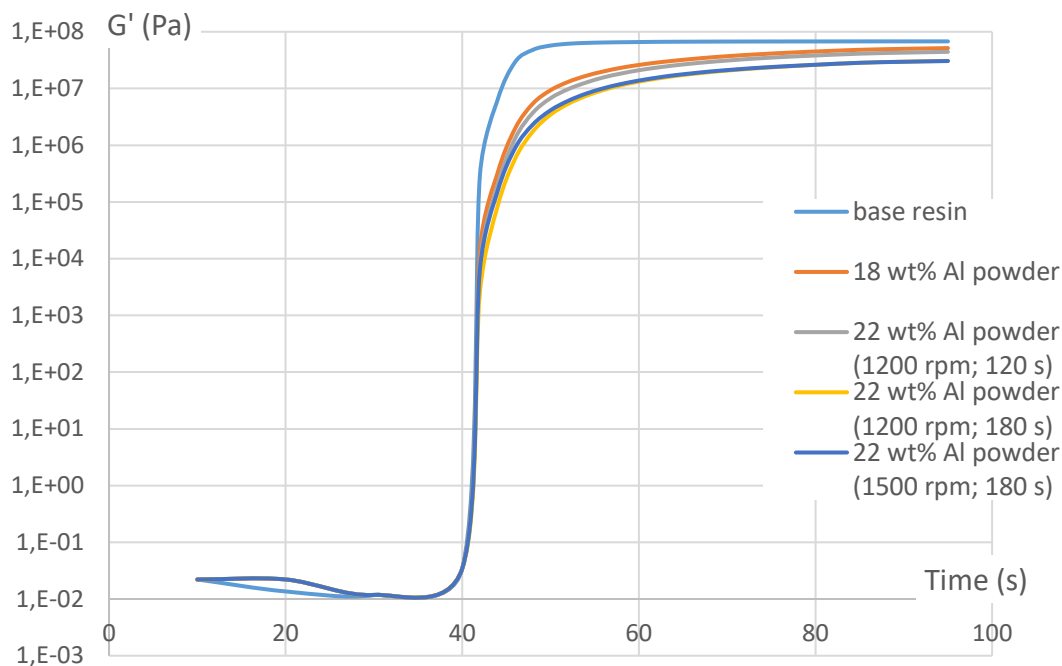


Figure 29. Photo-rheology curve of resin filled with AlSi10Mg powder

The graph in Figure 29 shows that, as expected, the higher filling ratio implies a slower polymerization. Moreover, also the final value of G' is lowered. Interestingly, the same happens increasing the mixing energy (in terms of mixing time or mixing revolution speed) indicating that the powder is not completely suspended until a certain level of energy is reached. This affects the concentration of the powder in the resin during sampling, because only suspended particles can be taken together with the resin. Therefore, the more the powder is well distributed in the resin, the closer the concentration of the sample to the mass ratio between resin and powder.

The effect of mixing energy is also evident from the cure depth measured with the micrometer reported in Table 2:

Table 2. Cure depth of a resin with increasing AlSi10Mg powder content

Sample	Cure Depth mm
base resin	0.99
18 wt% AlSi10Mg (1200 rpm; 60 s)	1.02
22 wt% AlSi10Mg (1200 rpm; 60 s)	0.89
22 wt% AlSi10Mg (1200 rpm; 180 s)	0.62
22 wt% AlSi10Mg (1500 rpm; 180 s)	0.57

Even though the cure depth is largely reduced, the thickness of the samples produced with the PR test is an order of magnitude higher than the one of a printing layer, that is in the order of a few tens of micrometers. This signifies that, having the same light source used in the printer, with proper exposure times, the production of components with metal filled resin using an MSLA process should be possible. However, the concentration of powder is still low to produce full dense parts and it is limited because of poor suspension stability.

A comparison between the effects of two different fillers has been given by the PR test of a suspension of Al₂O₃ powder in the same acrylic resin used with the aluminum powder. The same procedure has been followed and the results are reported in Figure 30:

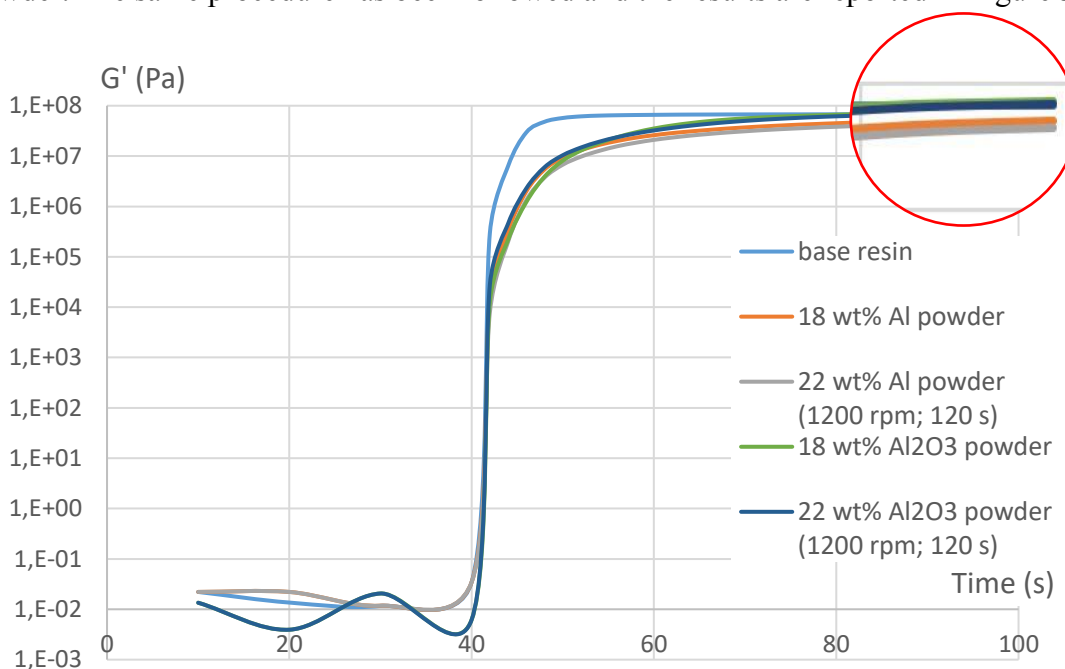


Figure 30. PR curves of resin filled with AlSi12Mg and Al₂O₃ powder

From the results of PR tests, the main perceived difference is the higher final level of G' that may be correlated to a deeper cure of the resin. To verify this hypothesis the cure depth has been measured with the micrometer and results are reported in Table 3:

Table 3. Cure depth of an Al₂O₃ powder filled resin with increasing mixing energy

Sample	Cure Depth mm
18 wt% Al ₂ O ₃ powder	1.00
22 wt% Al ₂ O ₃ powder (1200 rpm; 120 s)	1.00
22 wt% Al ₂ O ₃ powder (1200 rpm; 180 s)	1.02
22 wt% Al ₂ O ₃ powder (1500 rpm; 180 s)	1.00

Compared to the cure depth measured in Table 2, this result suggests that alumina powder absorbs less light than the aluminum alloy powder. Furthermore, the smaller mean particle size of the ceramic powder, is detrimental for the scattering phenomenon because, for the same weight percent, a higher number of particles are suspended in the resin. However, there is an important factor that must be considered: the density of alumina is significantly higher than the one of aluminum powder, therefore the volume fraction of the aluminum powder in the resin is higher than the volume fraction of the alumina powder.

It is possible to estimate the equivalent volume fraction of alumina with the following considerations: knowing that the mass density of the Al alloy $\rho_{AlSi} = 2650 \frac{kg}{m^3}$ and the mass density of alumina $\rho_{Al_2O_3} = 3950 \frac{kg}{m^3}$; for a given weight percent the ratio between the volume percentage of the two powders is equal to the ratio between the densities:

$$\frac{AlSi \text{ vol}\%}{Al_2O_3 \text{ vol}\%} = \frac{\rho_{Al_2O_3}}{\rho_{AlSi}} = 1.49$$

Therefore, considering 22 wt% of AlSi10Mg, a comparable amount of alumina filling ratio in terms of volume percentage is:

$$Al_2O_3 \text{ wt}\% = \frac{\rho_{Al_2O_3}}{\rho_{AlSi}} \cdot AlSi \text{ wt}\% = 33.8$$

These considerations can be taken into account when comparing the filling ratio of resin with different material: a lighter material requires lower mass concentrations to reach dense final parts.

4.2.2. Air pockets

We expect that air pockets negatively influence the curing of the resin and, to prove this, PR tests have been performed on vacuum mixed samples. In Figure 31, are shown the PR tests of the 22 wt% filled resin with metal powder. In the graph, there is an evident improvement in curing speed (especially in the last portion of the graph) and final level of G' for vacuumed samples. A similar trend has been shown by the test with the ceramic filled resin.

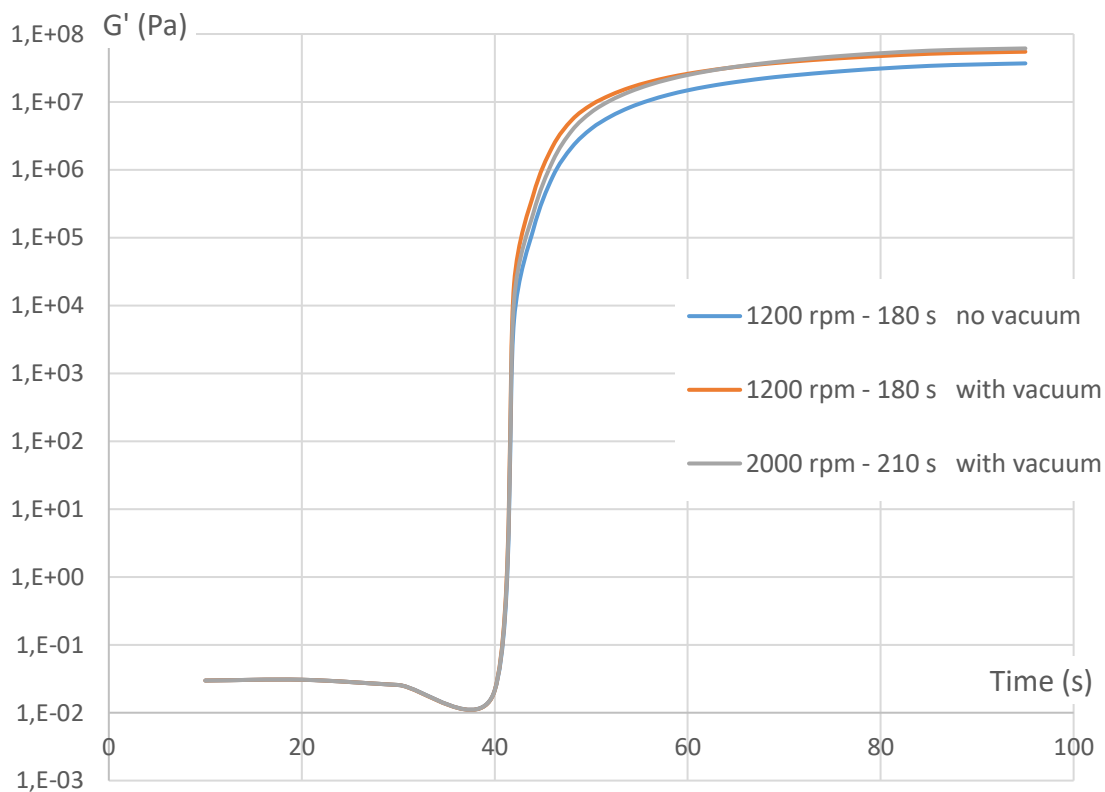


Figure 31. PR curves of vacuum mixed resin filled with AlSi10Mg particles

Also in this test, a higher final level of G' is correlated to a deeper polymerization (Table 4).

Table 4. Vacuum mixing effect on cure depth of filled resin

Sample	Cure Depth mm
1200 rpm - 180 s - no vacuum	0.80
1200 rpm - 180 s - with vacuum	0.98
2000 rpm - 210 s - with vacuum	0.92

In this case, the higher mixing energy has a double effect: increasing the mixing speed, a higher number of suspended particles reduces the cure depth; increasing the mixing time, instead, the vacuuming is performed in a more effective way. Undoubtedly, a better dispersion of particles has to be preferred despite the slightly lower cure depth.

After embedding the samples in epoxy resin, grinding and polishing, PR samples can be seen at the reflected light microscope. Here, the air pockets are seen as almost spherical, dark voids and can be clearly recognized by adjusting the focus to scan the pocket at different depth (Figure 32).

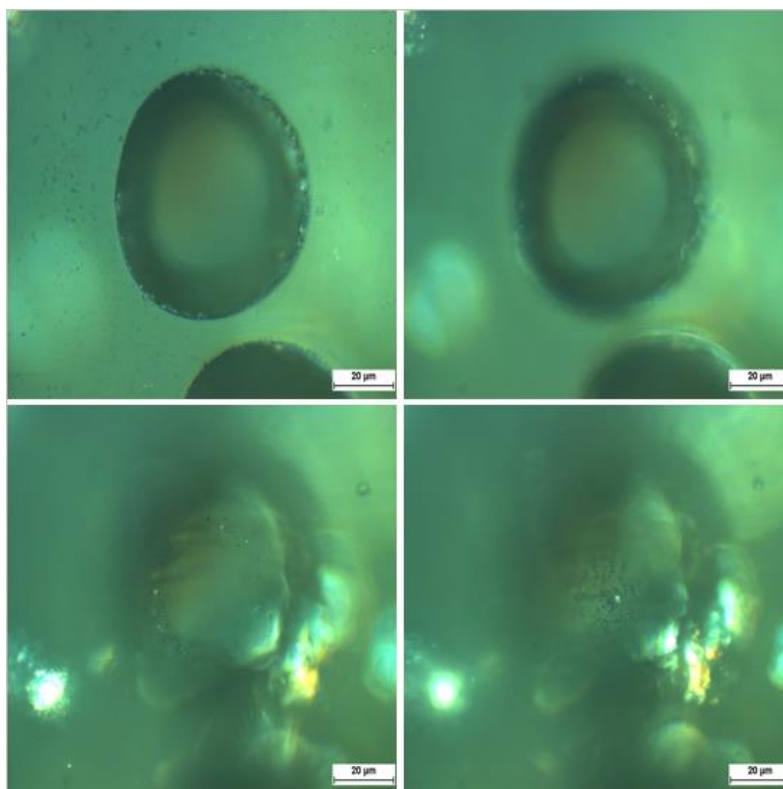


Figure 32. Micrograph of an air pocket with the focus at different depth

For the analysis of air pocket, it is useful to record videos that show the morphology of the pocket by smoothly varying the focus of the microscope.

As shown in Figure 33, the effect of vacuum mixing is noticeable at the microscope by looking at the section of a single cured layer (that is the PR cured sample after grinding and polishing).

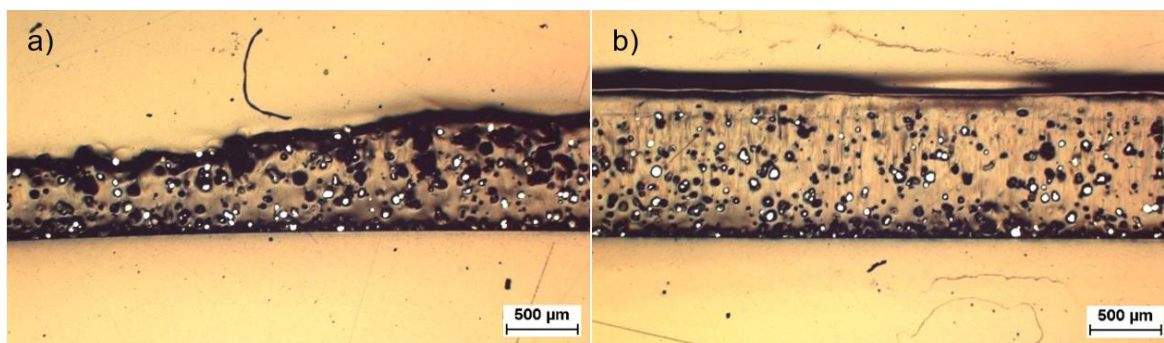


Figure 33. Single cured layer of filled resin mixed without (a) and with (b) vacuum

The clear improvement in curing kinetics with the vacuum mixing is noticed both because of the increase of the curing depth and because the sample was cured uniformly. Nonetheless, the vacuum mixing is not able to completely overcome the air trapping and many pockets are also detected in the vacuumed sample. To enhance the performance of polymerization of the resin, a defoamer for the system must be found. To this scope, some PR tests and some microscopy investigations have been done on samples with the defoamers suggested by the partner company BYK and listed in Table 5; however, the reduction of air trapping was not significant.

Table 5. Tested defoamers

Defoamers	composition
BYK-019	Solution of a polyether-modified polydimethylsiloxane
BYK-1790	Polyolefin
BYK-1799	Blend of hydrophobic solids and foam-destroying polysiloxanes

In Figure 33, the fast sedimentation of the powder can also be seen, i.e., the higher concentration of powder at the bottom surface with respect to the top surface.

4.3. Suspension stability and resin viscosity

The suspension stability and resin viscosity are contrasting factors for which the best compromise has to be found in the resin composition and additives. The settlement speed is related to the powder PSD, the powder and the resin densities and the resin formulation in terms of base composition (monomers and oligomers used) and the eventual addition of rheology additives.

4.3.1. Effect of different powders on sedimentation

The effect on sedimentation stability of different powders depends on the PSD, that has already been examined in 4.1.1, and the density. In Table 6, the densities for the different powder are reported:

Table 6. Powder densities

Powder	ρ kg/m ³
AlSi10Mg	2650
Al ₂ O ₃	3950
316L	8000
AlSi12	2650

The combined effect of PSD and density is examined at the reflected light microscope in a single cured layer and the micrographs are shown in Figure34, to Figure 36.

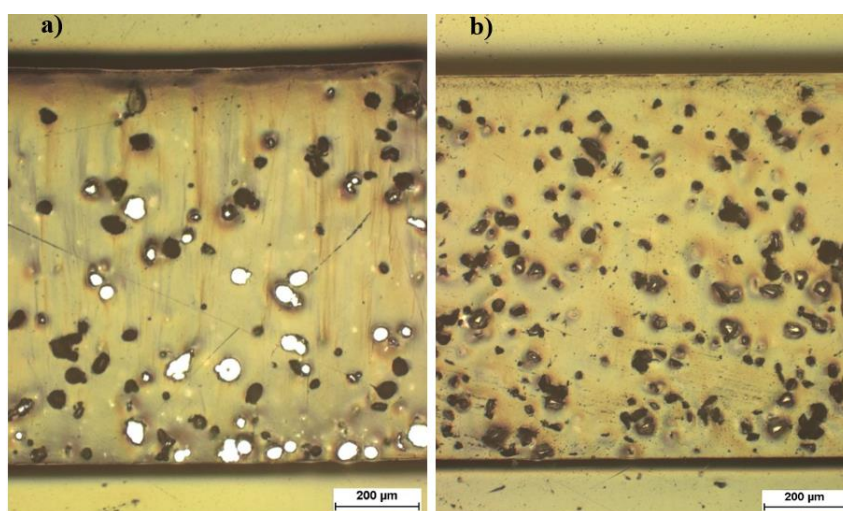


Figure 34. AlSi10Mg (a) and Al₂O₃ (b) powder suspension in acrylic resin

In Figure 34, the comparison between a resin filled with 22 wt% of AlSi10Mg and a resin filled with the 22 wt% of Al₂O₃ powder is made. Despite the higher density of the ceramic powder, a more stable suspension is achieved. Even if the difference in particle morphology can influence the suspension stability, the main contribution to this result is to be attributed to the smaller average size of the particles. As a matter of fact, in Figure 35 the suspension of AlSi12 particles appears to be drastically improved compared to the AlSi10Mg system even if the density of the particles is similar.

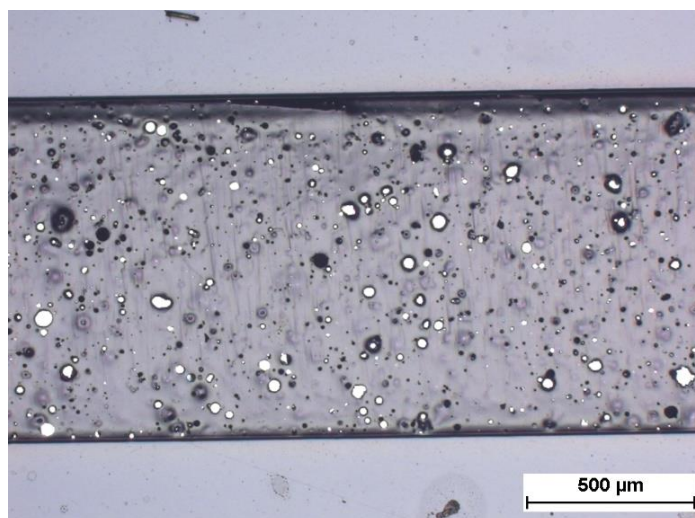


Figure 35. AlSi12 powder suspension in acrylic resin

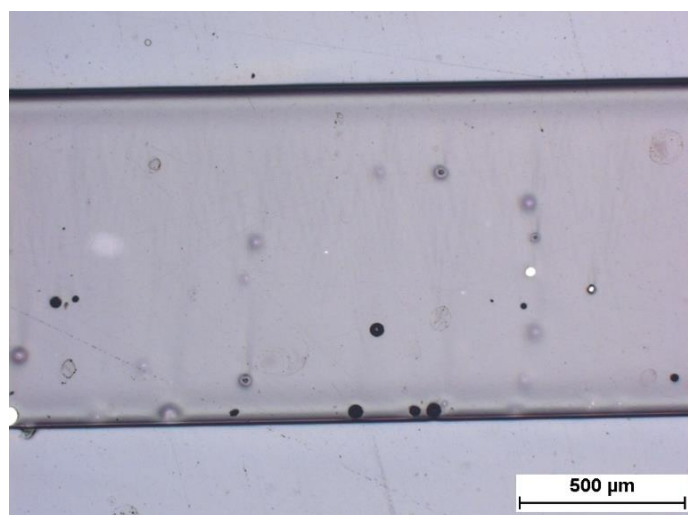


Figure 36. 316L powder sedimented in acrylic resin

In Figure 36, an unsuccessful trial of suspending stainless steel particles in acrylic resin is made. The high density of steel is considered to be the main cause of the fast sedimentation.

4.3.2. Rheology additives

Having established that the most stable suspension is given by the system filled with AlSi12 powder, the improvement of this system was achieved through the addition of dispersants in order to promote stabilization over a longer period of time making the resin suitable for SLA applications. The following additives provided by the company BYK were tested in this project:

- ANTITERRA-U100: salt of unsaturated polyamine amides and low-molecular acidic polyesters;
- CLAYTONE-APA: organophilic phyllosilicate;
- CLAYTONE-MPZ: specially modified organophilic phyllosilicate;
- DISPERBYK111: phosphoric acid ester;
- DISPERBYK180: alkyl ammonium salt of a copolymer with acidic groups;
- DISPERBYK2013: styrene maleic anhydride copolymer;
- GARAMITE-1210: organophilic phyllosilicates;
- GARAMITE-1958: organophilic phyllosilicates;
- RHEOBYK-430: solution of a high molecular weight, urea-modified, medium-polarity polyamide;
- RHEOBYK-7590: castor oil derivative.

For the sake of clarity, the effectiveness of the additive is reported in Table 7 and only the rheology curves of the most effective dispersants are described in this work.

Table 7. Effects of dispersants on suspension stability and viscosity

Dispersant	stability	viscosity
ANTITERRA-U100	low	low
CLAYTONE-APA	good	high
CLAYTONE-MPZ	medium	low
DISPERBYK111	low	low
DISPERBYK180	low	low
DISPERBYK2013	low	low
GARAMITE-1210	high	very high
GARAMITE-1958	high	very high
RHEOBYK-430	low	low
RHEOBYK-7590	good	very high

As shown in Table 7, the effectiveness in stabilization of suspension of a dispersant is always related to an increase in viscosity of the system; hence, a compromise between the two parameters has to be found. Since the highest power in terms of stabilization is given by the CLAYTON-APA, the GARAMITE-1210, the GARAMITE-1958 and the RHEOBYK-7590, the effect of these four dispersants on G' , G'' and viscosity is discussed. Due to the low differences in the behavior of GARAMITE-1210 and GARAMITE-1958, only the former is taken as a reference. The experiments are conducted incorporating the AlSi12 powder in an acrylic resin at a filling ratio equal to 30 wt% and then the dispersants are added incrementally. The concentration of all these four additives is given as a function of the powder mass following the recommendations of the supplier.

The amplitude sweep curves and the frequency sweep curves are reported in Figure 37 and Figure 38 respectively, and the flow curves are reported in Figure 39.

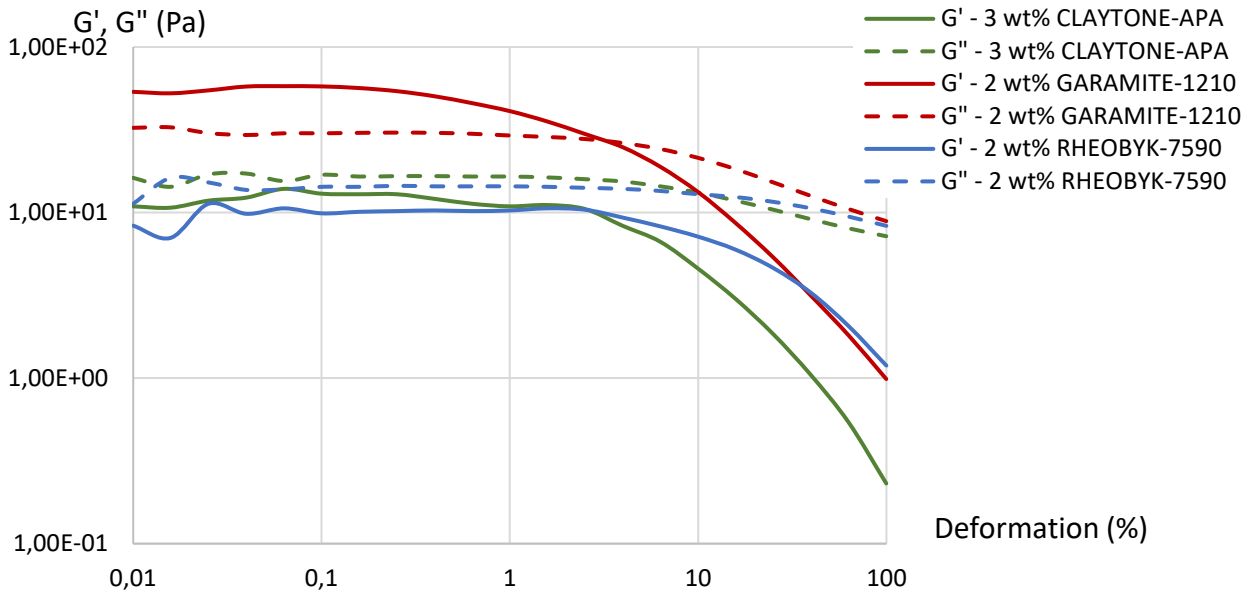


Figure 37. Amplitude sweep curves for different dispersants

The amplitude sweep curves highlight that the best stability in the low deformation region is provided by the GARAMITE-1210 (and GARAMITE-1958) since it is the only dispersant that is able to ensure a value of G' higher than G'' . However, also the other dispersants under investigation positively affect the storage and loss moduli by increasing the former to a level comparable to G'' .

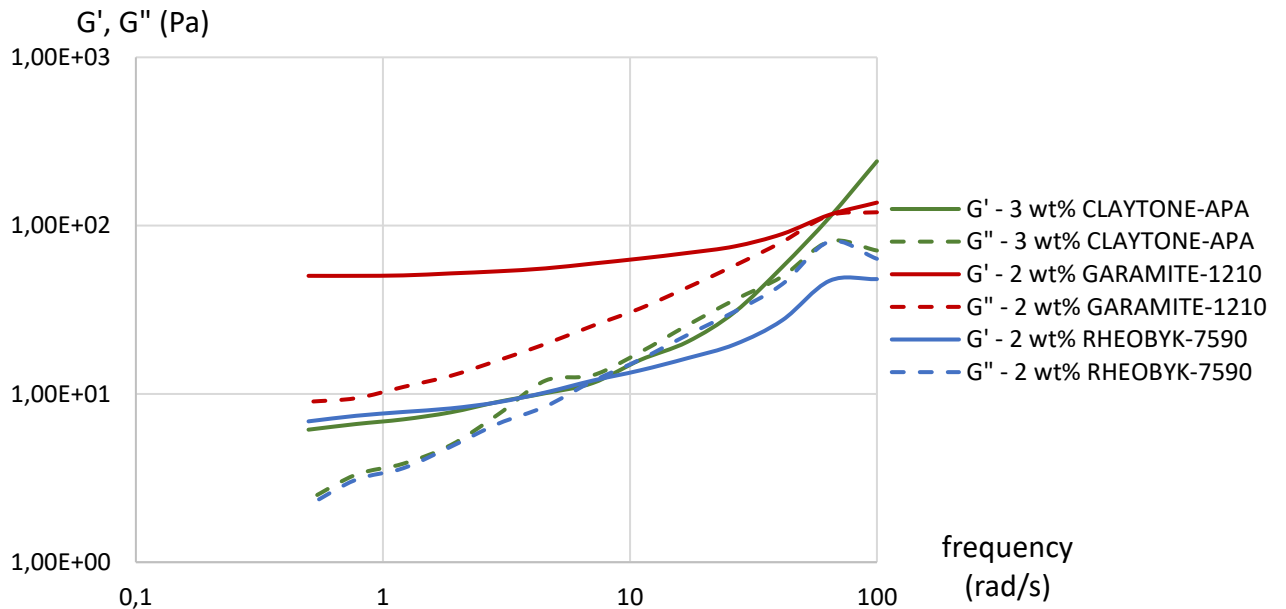


Figure 38. Frequency sweep curves for different dispersants

In the frequency sweep curves, all the additives favor stability of the system at low frequencies with the greatest improvement given by GARAMITE-1210/1958.

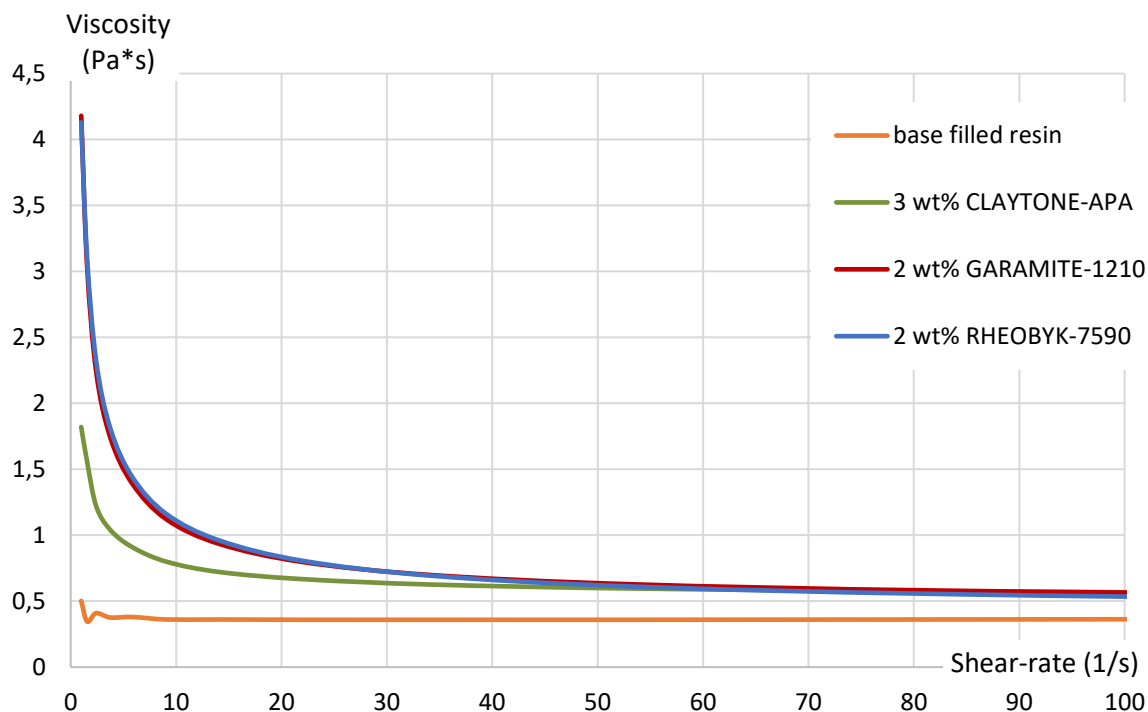


Figure 39. Viscosity vs shear-rate for filled resin with different dispersants

Flow curves in Figure 39 illustrate that the viscosity exponentially increases at low shear-rates when an effective dispersant is added to the resin.

Among all the tested dispersing additives, despite the tremendous increase of viscosity, the most suitable was found to be GARAMITE-1210 and GARAMITE-1958. An optimization procedure and the utilization of a booster can further improve the viscosity-stability trade-off.

4.3.3. Definition of an optimized formulation

The optimized resin formulation was identified starting with a base resin composed of a monomeric component (SR259 produced by Arkema) and an oligomer (LED9500 produced by WUX). The mass ratio between the two has been set to keep the viscosity of the base resin comparable to previous experiments:

$$\frac{m_{oligomer}}{m_{monomer}} = 0.363$$

The photoinitiator is not introduced yet since its influence on rheology is negligible. The powder filling ratio has been set in order to have approximately the equivalent volume content used for ceramic filled resin for SLA. Considering an Al_2O_3 wt% = 75 , then:

$$AlSi12 \text{ wt\%} = \frac{\rho_{AlSi12}}{\rho_{Al_2O_3}} \cdot Al_2O_3 \text{ wt\%} \approx 50$$

where ρ_{AlSi12} and $\rho_{Al_2O_3}$ are the densities of the aluminum alloy and the alumina respectively.

GARAMITE-1210 was chosen as the dispersant and two different boosters were evaluated.

Table 8. Boosters

Booster	composition
BYK-P 2720	Highly branched polymer amine
RHEOBYK-R 606	Polyhydroxy carboxylic acid ester

Following the recommendations of the supplier, the amount of booster was kept at an amount equal to 10% of the GARAMITE-1210 mass.

The optimization procedure was then based on tuning the GARAMITE-1210 content: increasing the dispersant content starting from 0.2 % with respect to the resin mass up to the level at which the level of G' was higher than G'' both in amplitude and frequency sweep curves. The results in terms of amplitude and frequency sweep are reported in Figure 40 and Figure 41 respectively. In Figure 42 the flow curves are reported.

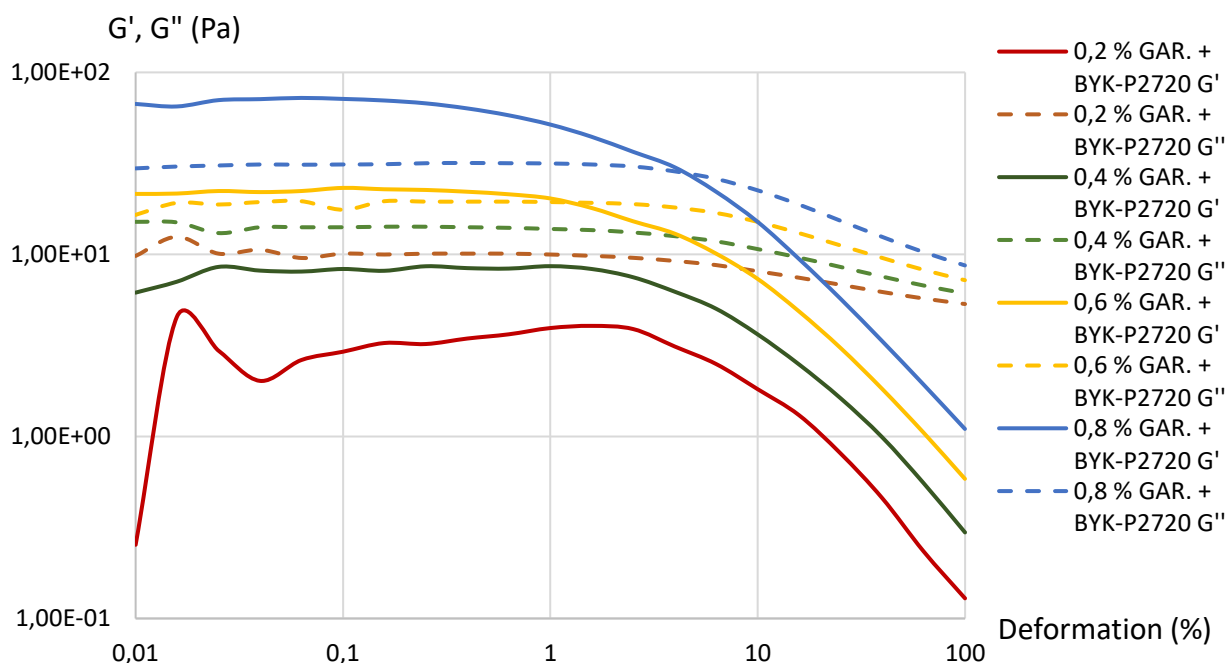


Figure 40. Amplitude sweep curves for the optimized resin with BYK-P2720

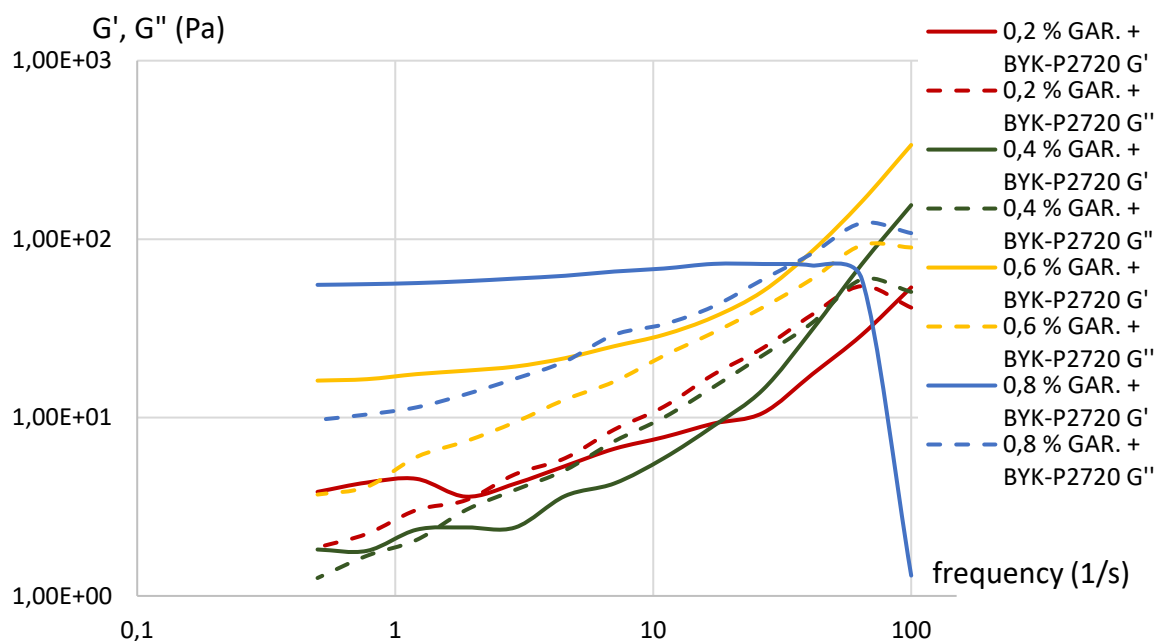


Figure 41. Frequency sweep curves for the optimized resin with BYK-P2720

As shown by the amplitude and frequency sweeps, the GARAMITE-1210 concentration has been raised up to 0.8%. At these values of dispersant concentration and filling ratio, the stability of the system was satisfactory. Similar results were achieved using the

RHEOBYK-R 606 instead of the BYK-P 2720 as a booster; however, slightly lower difference between G' and G'' was reached.

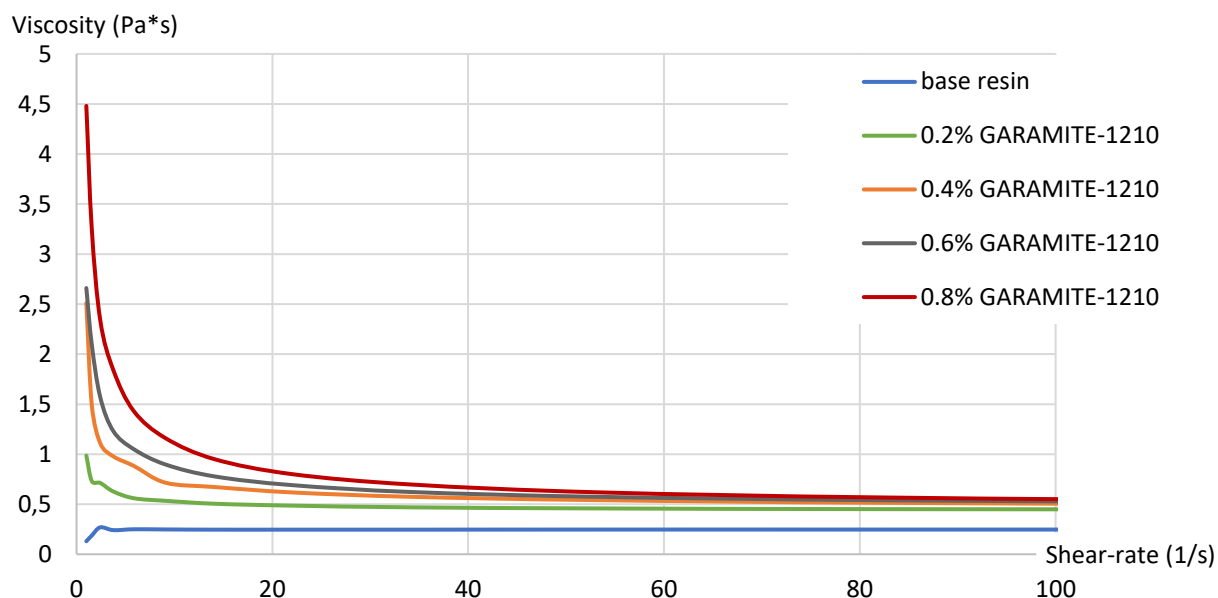


Figure 42. Viscosity vs shear-rate tuning the GARAMITE-1210 content

Figure 42 highlights that, despite a steep increase in the low shear-rate range, the viscosity of the filled resin with optimized GARAMITE-1210 and booster content is still in the printable range.

Therefore, the final optimized composition was made of:

- Base resin: composed of a monomer and an oligomer with a mass ratio of 0.363;
- AlSi12 powder with a filling ratio equal to 50 wt% with respect to the base resin;
- GARAMITE-1210: 0.8 wt% with respect to the powder content;
- BYK-P2720: 10 wt% with respect to the GARAMITE-1210.

Finally, the addition of BAPO produced by Rahn AG (photoinitiator) has been done before using the resin for SLA printing. The amount of PI was approximately 0.5 wt% with respect to the base resin.

4.4. Optimization of printing parameters

The optimization of printing parameters is an experimental procedure. All the parameters described in 3.4 are tuned to reach a proper adhesion of the part to the platform and

between layers and, at the same time, to minimize printing time. After multiple attempts, the printing parameters to produce solid components have been found (Table 9).

Table 9. Optimized printing parameters

Main printing parameters:	
1 st layer exposure time	200 s
Exposure time	4 s
Layer height	35-50 μm
Tilt time	5 s

With these parameters, some thin components have been produced, embedded in epoxy resin, grinded and polished to evaluate the layer formation and its morphology. Micrographs of embedded green bodies are reported in Figure 43, Figure 44 and Figure 45.

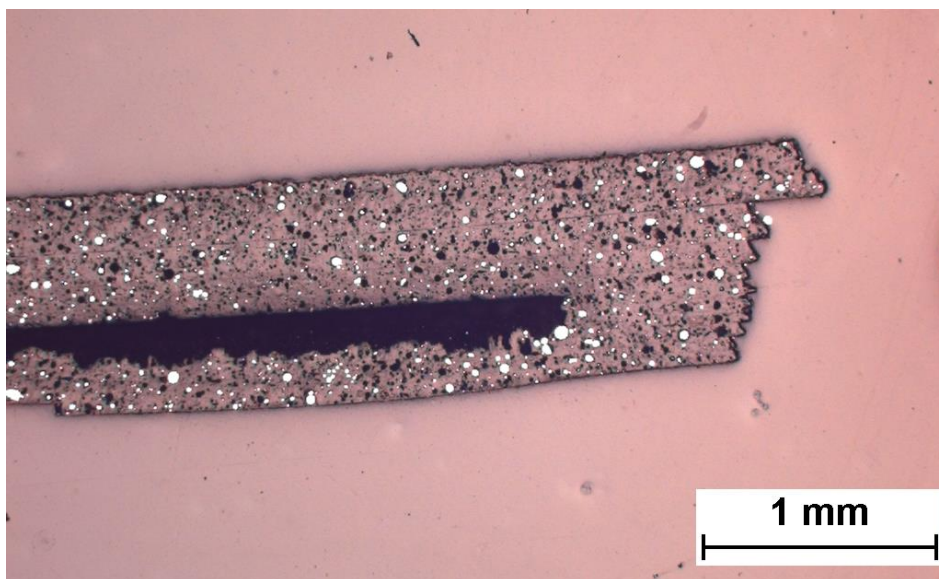


Figure 43. Micrograph of a printed part made of multiple layers

Figure 43 highlights interesting features of the printed component. First of all, the presence of the dark region at the interface between two layers may imply that the layer adhesion was weak or that the resin was not able to flow during the vat tilt, leaving a portion of the LCD screen not covered. This phenomenon suggests that an increase of exposure time or an improvement of the resin curability is needed to increase cure depth

and a lower viscosity of the resin is to be preferred to facilitate the flow caused by the vat tilt movement.

Furthermore, the sawtooth profile of the part (Figure 44) highlights the effect of scattering. As a matter of fact, the side of a layer in contact with the FEP film is wider than the side in contact with the platform or a previously cured layer.

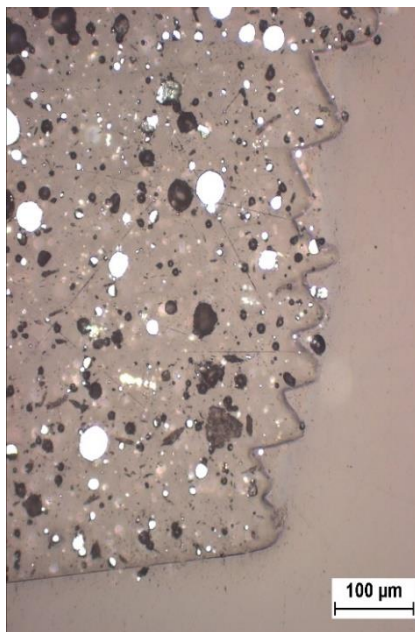


Figure 44. Micrograph of the sawtooth profile of a printed part

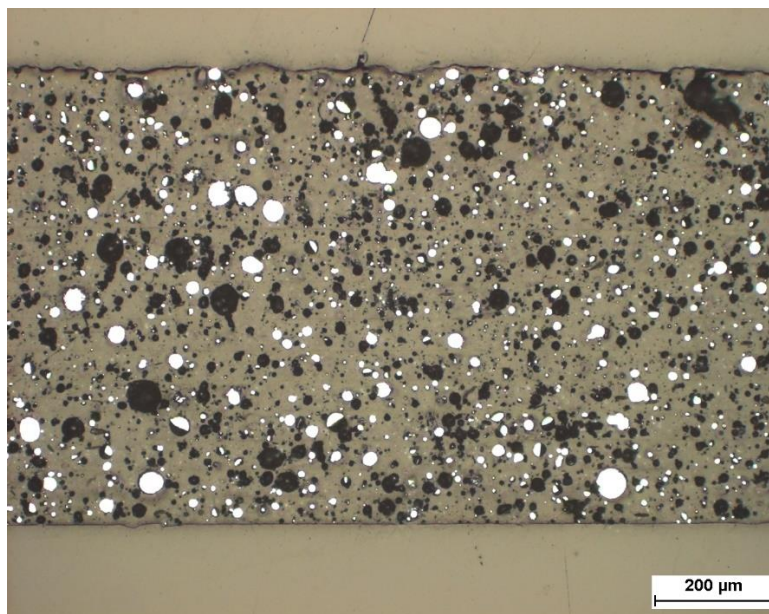


Figure 45. Micrograph of a printed part

In Figure 45, the printed part shows very good dispersion of particles demonstrating the stabilizing capabilities of GARAMITE-1958. Furthermore, a good layer adhesion is evidenced from apparently seamless interlaminar adhesion. This means that the through cure was sufficient to join the layers properly.

However, the presence of air pockets is still evident even after vacuum centrifugal mixing of the resin. This is caused by the poor control of air trapping during pouring of the resin in the vat and during the printing process. Reducing the air trapping phenomenon could allow the usage of lower exposure times leading to higher throughput and lower necessity of long-term sedimentation stability.

4.5. Debinding and sintering

Debinding and sintering for ceramic parts is performed in a unique step in a furnace, however, due to the high affinity of aluminum with oxygen, the sintering of Al alloys requires furnaces with a controlled environment. Despite the limitation of the oxidizing environment, some attempt to debind some thin printed parts have been made (Figure 46).

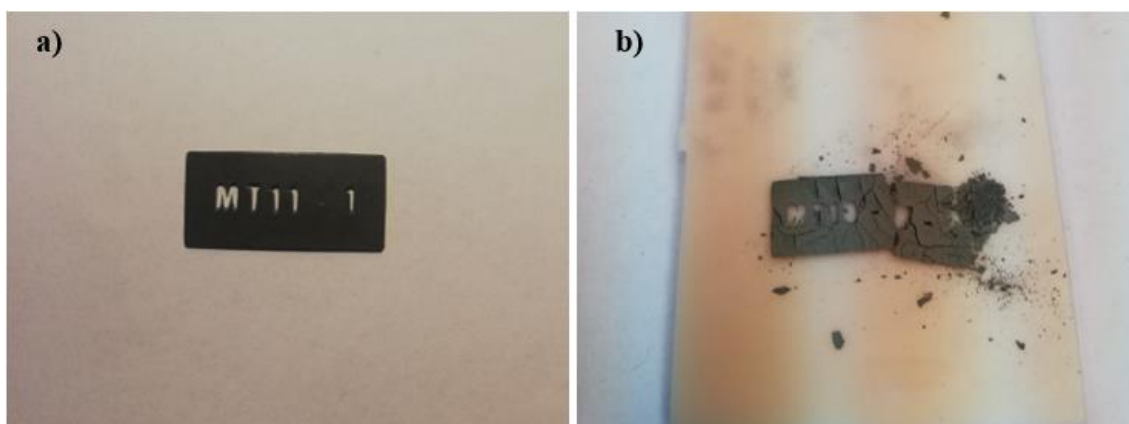


Figure 46. Green part (a) and debinded part in oxidizing environment (b)

As expected, the debinded part resulted in oxidized powder. Interesting considerations, however, can be made by analyzing brown bodies with different filling ratio. Since the debinding phase is used to remove the polymeric binder, i.e., the resin, from the green body, we can expect that the higher the filling ratio, the lower the shrinkage after debinding, and therefore also after sintering (Figure 47).

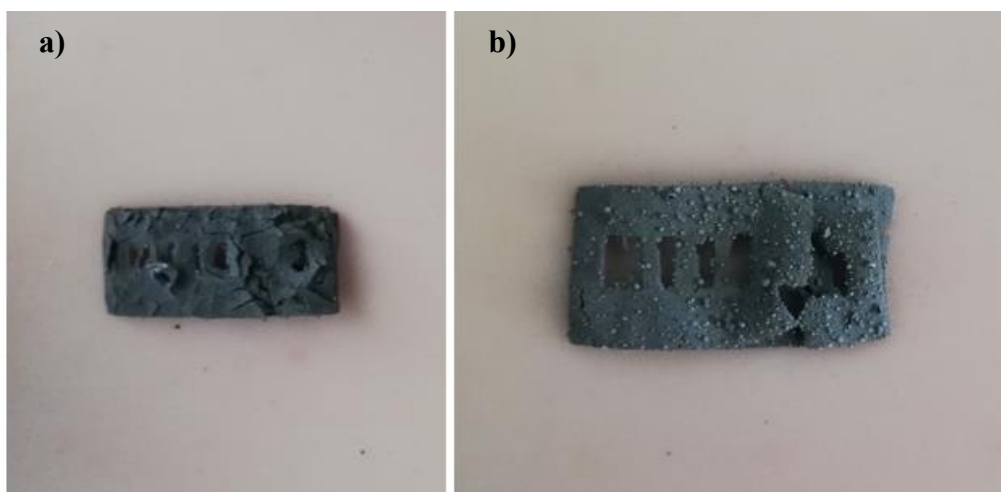


Figure 47. Brown bodies with filling ratios equal to 30 (a) and 50 (b) wt%

As expected, the higher powder content resulted in lower shrinkage after debinding. The average shrinkage of the parts is reported in Table 10.

Table 10. average shrinkage of parts after debinding for different filling ratio

AlSi12 content	Average Shrinkage
50 wt%	33.1
39 wt%	39.7
30 wt%	44.1

It is noticeable that the shrinkage is largely reduced with increasing powder content, however its value is considerably high. A scaling factor in the design of the part is required to compensate for the reduction in size and it must take into account the filler content in the resin. As a matter of fact, starting with green bodies of the same dimensions, shrinkage of parts during debinding ranged between 33.1% and 44.1% for parts filled with 50 wt% and 30 wt% of AlSi12 powder respectively.

5. Conclusion

In this work an experimental procedure is performed to define the composition of a resin filled with Al powder suitable for MSLA and to tune the printing parameters for the production of defect-free green bodies.

The characterization of different powders is done and their effect on resin stability and curing kinetics is analyzed with rheology and photo-rheology tests. The effects on stability and polymerization resulted to be directly related to the mass density and to the PSD with lighter particles that promote suspension stability and together with smaller particle size. Higher values of mean particle size are detrimental for the sedimentation phenomenon but improve curing speed and curing depth.

The effect of air trapping is investigated, and air pockets are reduced with a vacuum mixer to minimize the adverse effect on polymerization. BYK-019, BYK-1790 and BYK-1799 have been tested as defoaming additives with negligible results.

The stabilization of the suspension is achieved with the introduction of dispersing agents, in particular GARAMITE-1210 and GARAMITE-1958. The viscosity of the resin is negatively affected by the addition of effective dispersants; therefore, the boosters BYK-P 2720 and RHEOBYK-R 606 are added to the composition to enhance the stabilizing effect and minimize the viscosity increase. A stable composition with a viscosity in the printable range has been reached for an acrylic base resin composed of SR259 and LED9500 as monomeric and oligomeric components and BAPO as photoinitiator.

After the tuning of printing parameters, the filled resin with optimized composition resulted to be suitable for defect free MSLA green bodies. The as-printed parts have been investigated with a reflected light microscope to detect defects and peculiarities.

Consideration of brown parts produced in oxidizing environment are made and the shrinkage during debinding is measured for green bodies with different filling ratio.

The tests conducted have demonstrated that metal-filled resins are a viable path for the production of green parts with MSLA and a good opportunity to extend the variety of processable metals with AM and introduce an alternative AM technique.

References

1. ISO/ASTM 52900. Standard Terminology for Additive Manufacturing – General Principles – Terminology. ASTM International (2022)
2. Atzeni, E.: AM basic concepts. Additive and design for additive, Turin, 2021
3. Galati, M., Minetola, P.: Analysis of Density, Roughness, and Accuracy of the Atomic Diffusion Additive Manufacturing (ADAM) Process for Metal Parts. *Materials* (Basel, Switzerland) **12**(24) (2019). doi: 10.3390/ma12244122
4. Desktop Metal, Inc.: Deep Dive: Bound Metal Deposition (BMD)
5. Markforged: What is Atomic Diffusion Additive Manufacturing (ADAM)?
6. Ayre, M.: Design guidelines for Direct Metal Laser Sintering (DMLS). *Crucible design* (2015)
7. Atzeni, E.: AM processes for metals. Additive and design for additive, Turin, 2021
8. Gruber, S., Grunert, C., Riede, M., López, E., Marquardt, A., Brueckner, F., Leyens, C.: Comparison of dimensional accuracy and tolerances of powder bed based and nozzle based additive manufacturing processes. *Journal of Laser Applications* **32**(3), 32016 (2020). doi: 10.2351/7.0000115
9. Valdivieso, C.: The Complete Guide to Directed Energy Deposition (DED) in 3D Printing (2019)
10. Gonzalez-Gutierrez, J., Cano, S., Schuschnigg, S., Kukla, C., Sapkota, J., Holzer, C.: Additive Manufacturing of Metallic and Ceramic Components by the Material Extrusion of Highly-Filled Polymers: A Review and Future Perspectives. *Materials* (Basel, Switzerland) **11**(5) (2018). doi: 10.3390/ma11050840
11. La tecnologia HP Metal Jet. Documentazione Tecnica (2018)
12. Kodama, H.: Automatic method for fabricating a three-dimensional plastic model with photo-hardening polymer. *Review of Scientific Instruments* **52**(11), 1770–1773 (1981). doi: 10.1063/1.1136492
13. Hull, C.W.: Apparatus for production of three-dimensional objects by stereolithography Patent 4,575,330, 11 March 1986
14. Schmidleithner, C., Kalaskar, D.M.: Stereolithography. In: Cvetković (Ed.) 2018 – 3D Printing, IntechOpen
15. Au, A.K., Huynh, W., Horowitz, L.F., Folch, A.: 3D-Printed Microfluidics. *Angew. Chem.* **128**(12), 3926–3946 (2016)

16. Yang, Y., Loh, H.T., Fuh, J., Wang, Y.G.: Equidistant path generation for improving scanning efficiency in layered manufacturing. *Rapid Prototyping Journal* **8**(1), 30–37 (2002). doi: 10.1108/13552540210413284
17. Atzeni, E.: *AM processes for polymers. Additive and design for additive*, Turin, 2021
18. Weng, Z., Zhou, Y., Lin, W., Senthil, T., Wu, L.: Structure-property relationship of nano enhanced stereolithography resin for desktop SLA 3D printer. *Composites Part A: Applied Science and Manufacturing* **88**, 234–242 (2016). doi: 10.1016/j.compositesa.2016.05.035
19. Takada, K., Sun, H.-B., Kawata, S.: Improved spatial resolution and surface roughness in photopolymerization-based laser nanowriting. *Appl. Phys. Lett.* **86**(7), 71122 (2005)
20. Lumi Industrues 3D solutions: *La guida definitiva alle tecnologie di stampa 3D a resina* (2019)
21. Sun, C., Fang, N., Wu, D.M., Zhang, X.: Projection micro-stereolithography using digital micro-mirror dynamic mask. *Sensors and Actuators A: Physical* **121**(1), 113–120 (2005)
22. Parenti, M.: *DLP vs LCD 3D Printer: The Main Differences* (2022)
23. Carbon, Inc.: *What is Carbon Digital Light Synthesis?*
24. Voet, V.S.D., Strating, T., Schnelting, G.H.M., Dijkstra, P., Tietema, M., Xu, J., Woortman, A.J.J., Loos, K., Jager, J., Folkersma, R.: Biobased Acrylate Photocurable Resin Formulation for Stereolithography 3D Printing. *ACS omega* **3**(2), 1403–1408 (2018). doi: 10.1021/acsomega.7b01648
25. Andrzejewska, E., Andrzejewski, M.: Polymerization kinetics of photocurable acrylic resins. *J. Polym. Sci. A Polym. Chem.* **36**(4), 665–673 (1998). doi: 10.1002/(SICI)1099-0518(199803)36:4<665:AID-POLA15>3.0.CO;2-K
26. Fouassier, J., Allonas, X., Burget, D.: Photopolymerization reactions under visible lights: principle, mechanisms and examples of applications. *Progress in Organic Coatings* **47**(1), 16–36 (2003). doi: 10.1016/S0300-9440(03)00011-0
27. Bartolo, P.J., Gaspar, J.: Metal filled resin for stereolithography metal part. *CIRP Annals* **57**(1), 235–238 (2008). doi: 10.1016/j.cirp.2008.03.124
28. G. Allen Brady, Tien-Min Chu, John W. Halloran: *Curing Behavior of Ceramic Resin for Stereolithography*
29. Bhattacharjee, S.: DLS and zeta potential - What they are and what they are not? *Journal of controlled release : official journal of the Controlled Release Society* **235**, 337–351 (2016). doi: 10.1016/j.jconrel.2016.06.017

30. Byk: Dispersing additives

31. Navlani-García, M., Salinas-Torres, D., Mori, K., Kuwahara, Y., Yamashita, H.: Tailoring the Size and Shape of Colloidal Noble Metal Nanocrystals as a Valuable Tool in Catalysis. *Catal Surv Asia* **23**(3), 127–148 (2019). doi: 10.1007/s10563-019-09271-7

Acknowledgment

I dutifully thank all the people of the IFKB who welcomed me and helped me throughout my stay in Stuttgart. Special thanks to Wadih, who devoted himself with great involvement to the work we did at the institute and made this project possible; to Yilmaz, who followed the project with great interest; and to Mr Frank Abschlag from BYK, who supported the experiments with precious consultancy. I thank Professor Atzeni who believed in this project and allowed me to take part in Erasmus experience.

I also thank all the people I met in Stuttgart outside the institute who made me enjoy my stay in Germany and introduced me to different cultures.